

# Effects of $\pi$ -spacer and fluorine loading on the optoelectronic and photovoltaic properties of (X-DADAD)<sub>n</sub> benzodithiophene-based conjugated polymers



Alexander V. Akkuratev<sup>a,\*</sup>, Ilya E. Kuznetsov<sup>a</sup>, Petr M. Kuznetsov<sup>a</sup>, Nikita V. Tukachev<sup>a</sup>, Ilya V. Martynov<sup>a</sup>, Sergey L. Nikitenko<sup>a</sup>, Artyom V. Novikov<sup>a,b</sup>, Alexander V. Chernyak<sup>a</sup>, Andriy Zhugayevych<sup>b</sup>, Pavel A. Troshin<sup>b,a</sup>

<sup>a</sup> Institute for Problems of Chemical Physics of the Russian Academy of Sciences (IPC RAS), Academician Semenov avenue 1, Chernogolovka, Moscow region, 142432, Russian Federation

<sup>b</sup> Skolkovo Institute of Science and Technology, Nobel st. 3, Moscow, 143025, Russian Federation

## ARTICLE INFO

**Keywords:**  
Conjugated polymers  
Benzothiadiazole  
Thiophene  
Benzodithiophene  
Organic solar cells

## ABSTRACT

Four new conjugated polymers based on benzodithiophene, thiophene and 2,1,3-benzothiadiazole or 5,6-difluoro-2,1,3-benzothiadiazole were synthesized and investigated as absorber materials for organic photovoltaics. The effect of (bi)thiophene  $\pi$ -spacers and fluorine substitution on the physicochemical and optoelectronic properties of the polymers was revealed and correlations were drawn with their electrical characteristics in organic solar cells. In particular, introducing either thiophene spacers or fluorine substituents does not affect much the photovoltaic performance of the polymers, while the combination of both routes was found to be a promising strategy for improving the charge carrier mobilities and morphology of the polymer-fullerene blends as well as light power conversion efficiency in solar cells based on these materials. The bulk heterojunction organic solar cells based on the  $\pi$ -bridged and fluorinated polymer P4 showed the highest short-circuit current density and power conversion efficiency of 7 %, which is an inspiring value for fullerene-based organic photovoltaics. Most importantly, our findings provide important insights into rational design of high-performance conjugated polymers while pursuing a combination of two efficient backbone functionalization strategies based on introduction of fluorine substituents and  $\pi$ -spacers to control the geometry and electronic characteristics of the polymer chains.

## 1. Introduction

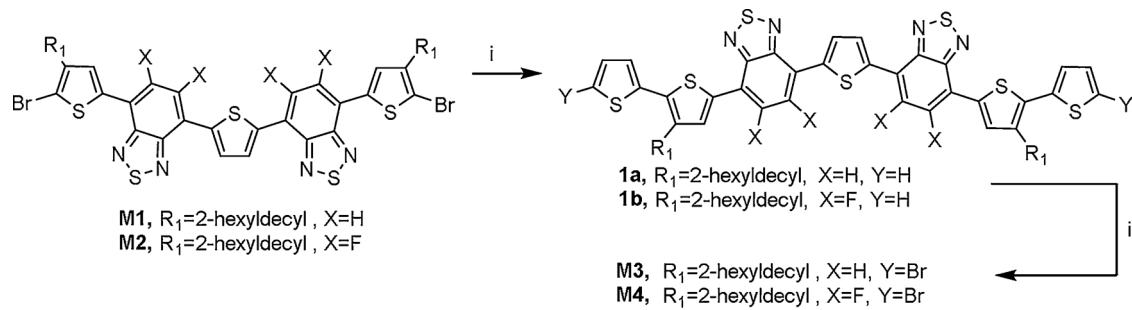
Organic solar cells (OSCs) are actively investigated over the past two decades due to their potential to become lightweight, flexible and low cost source of solar energy for a broad range of applications [1]. The power conversion efficiency (PCE) of OSCs depends mainly on the properties of the materials used in the active layer, e.g. conjugated polymers. Various approaches are currently implemented to design high performance conjugated polymers for photovoltaic applications [2–6]. Incorporation of alternating electron donor (D) and electron acceptor (A) moieties into the polymer backbone represents one of the most widely used strategies to design absorber materials with tailored optical and electronic properties. In particular, this so-called “push-pull” approach allows one to control frontier energy levels, band gap, charge carrier mobility of conjugated polymers as well as nanoscale

morphology of their blends with acceptor components.

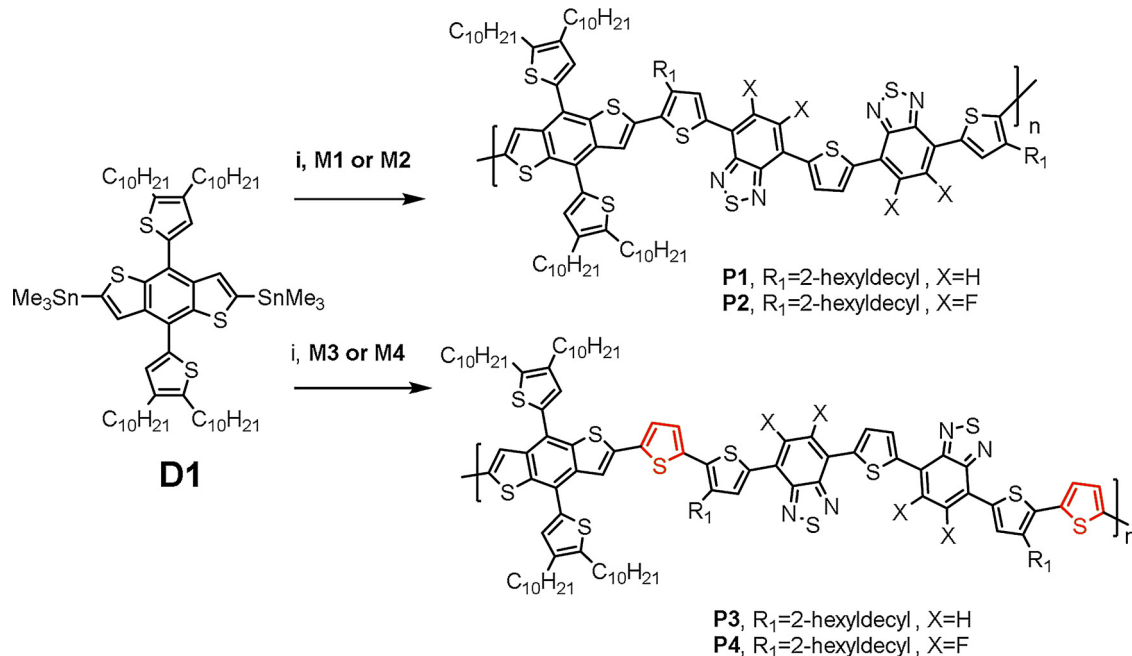
Within the last years, a particular attention is paid to the introduction of electron-withdrawing fluorine substituents in the polymer backbone while modifying either donor or acceptor units or even both of them [7]. Fluorine substitution was shown to be an efficient approach to optimize the optoelectronic properties of conjugated polymers, e.g. by lowering HOMO energy and thus enhancing the open-circuit voltage ( $V_{OC}$ ) of organic solar cells [8–12]. Moreover, introduction of the fluorine atoms makes polymers less miscible with acceptor counterparts thus suppressing the formation of disordered mixed phases contributing strongly to the recombination of charge carriers [13]. Thus, using fluorine-loaded polymers improves active layer morphology and photovoltaic performance (mainly due to increased current density) owing to the blocked loss channel. Di-fluorobenzothiadiazole represents one of the most popular fluorine-

\* Corresponding author.

E-mail address: [akkuratev@yandex.ru](mailto:akkuratev@yandex.ru) (A.V. Akkuratev).



**Scheme 1.** Synthesis of the monomers **M1-M4**. Conditions: i - tributyl(thiophen-2-yl)stannane,  $\text{Pd}(\text{PPh}_3)_4$ , toluene, reflux; ii - *N*-bromosuccinimide, 1,2-dichlorobenzene.



**Scheme 2.** Synthesis of conjugated polymers **P1-P4**. Conditions: i –  $\text{Pd}_2(\text{dba})_3$ ,  $(4\text{-MeC}_6\text{H}_5)_3\text{P}$ , toluene, reflux.

**Table 1**

Physicochemical and optoelectronic properties of polymers **P1-P4**.

	$\text{M}_w$ , kDa	$\text{M}_w/\text{M}_n$	$T_d$ , °C	$T_m/T_c$ , °C	$E_{\text{onset}}^{\text{ox}}$ , V vs. $\text{Fc}^+/\text{Fc}$	HOMO/ LUMO <sup>a</sup> , eV	$\lambda_{\text{max}}^{\text{b}}$ , nm	$\lambda_{\text{max}}^{\text{c}}$ , nm	$E_g$ , eV
P1	152	1.6	449	249/217	0.58	-5.68/-4.01	606	644	1.67
P2	134	1.5	444	243/272	0.61	-5.71/-3.98	602	610	1.73
P3	168	1.5	380	–	0.37	-5.47/-3.84	538	628	1.63
P4	235	2.2	433	–	0.41	-5.51/-3.85	623	624	1.66

<sup>a</sup>  $E_{\text{LUMO}} = E_{\text{HOMO}} + E_g^{\text{opt}}$ .

<sup>b</sup> In 1,2-dichlorobenzene solution.

<sup>c</sup> In thin film.

containing building blocks for conjugated copolymers due to its availability, high photostability and attractive optoelectronic properties [14,15].

The introduction of additional  $\pi$ -spacers between the D and A units is commonly used to modulate and optimize planarity of the conjugated backbone, aggregation behavior of polymeric chains and miscibility of the electron donor polymers with the acceptor counterparts, e.g. fullere derivatives [16–22]. Conjugated  $\pi$ -spacers crucially affect the geometry of the macromolecules and hence their optical, electrochemical, charge transport and photovoltaic properties [23].

In our previous works, we reported the design of  $(\text{X-DADAD})_n$  conjugated polymers with the extended DADAD donor-acceptor molecular framework. These polymers demonstrate considerably improved

optoelectronic properties as compared to the well-known and easily accessible  $(\text{X-DAD})_n$  structures [24]. Moreover,  $(\text{X-DADAD})_n$  polymers usually demonstrate good photostability comparable to that of PCDTBT known as one of the most robust conjugated polymers [25,26]. According to the Scharber theoretical model, this type of donor materials with optimal optoelectronic properties can provide 13–15% efficiency in single-junction OSCs [27].

In this work, we synthesized four novel  $(\text{X-DADAD})_n$  polymers based on benzodithiophene (X), thiophene (D), and benzothiadiazole (A) units and investigated the effects of the thiophene  $\pi$ -spacer and fluorine loading in the polymer backbone on the optoelectronic and photovoltaic properties of the designed materials. The aim of the study was to evaluate the effects of each of the aforementioned modifications and

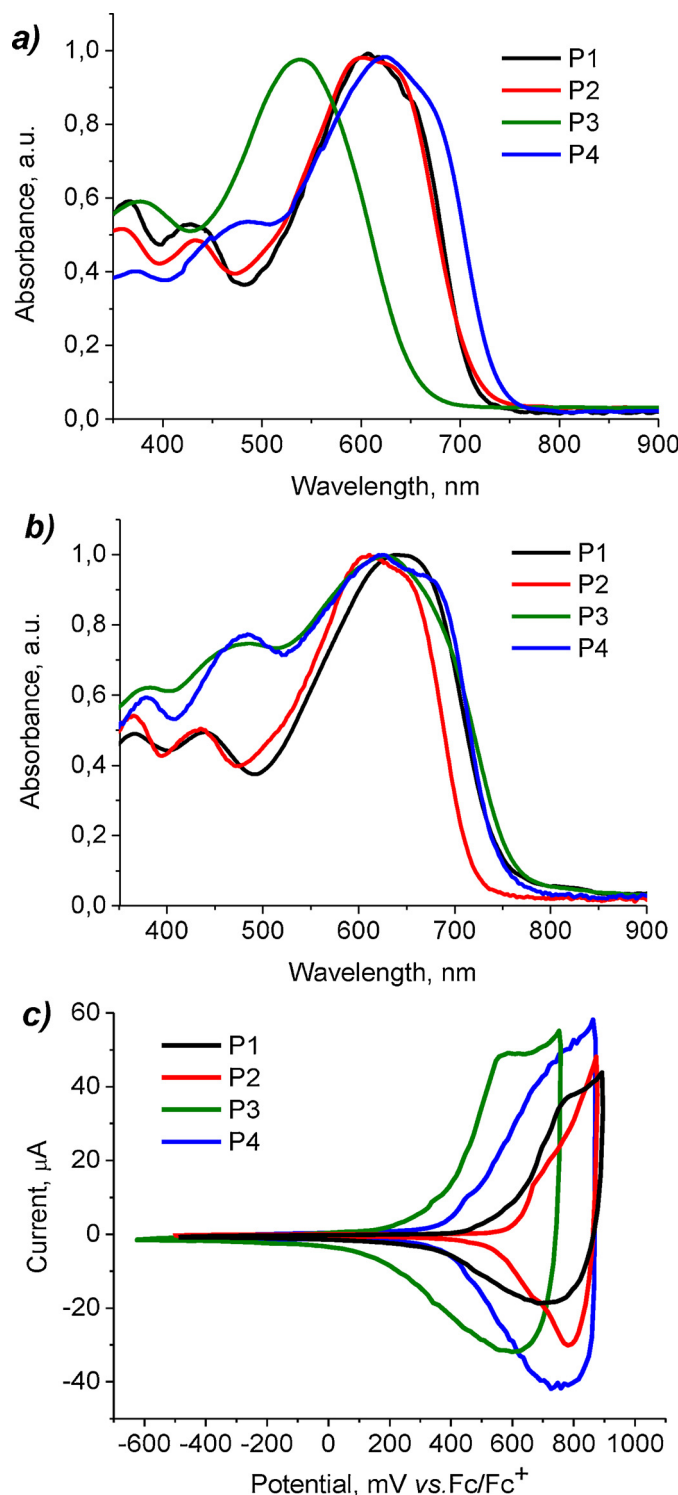


**Fig. 1.** Absorption spectra of polymers **P1–P4** in solution (**a**) and in thin films (**b**). Cyclic voltammograms for thin polymer films (**c**).

find a proper balance to enable further rational design of promising materials for efficient and stable organic photovoltaics.

## 2. Results and discussion

The synthesis of key monomers is shown in **Scheme 1**. Briefly, compounds **1a** and **1b** were prepared using Stille cross-coupling reactions between the monomers **M1** or **M2** [28,29] and tributyl(thiophen-2-yl)stannane (i). Further bromination of **1a–b** with *N*-

bromosuccinimide (ii) in 1,2-dichlorobenzene afforded the monomers **M3** and **M4**.

Conjugated polymers **P1–P4** were synthesized via palladium-catalyzed (i) Stille polycondensation reaction using monomers **M1–M4** and **D1** (**Scheme 2**). The synthesis of **D1** was reported previously [30].

The resulting polymers were precipitated with methanol and purified in Soxhlet apparatus by extraction with acetone, hexane, dichloromethane, and finally with chlorobenzene. The molecular weights of polymers were measured by gel permeation chromatography (GPC) as described previously [31]. All polymers possess high weight-average molecular weights ( $M_w$ ) ranging from 134 to 235 kDa and low polydispersity indexes ( $M_w/M_n$ ) of 1.5–2.2 (Table 1).

Thermal properties of conjugated polymers were studied by thermal gravimetry (TGA) and differential scanning calorimetry (DSC) in inert atmosphere ( $N_2$ ) with a heating rate of 15 °C/min. TGA and DSC curves are shown in Fig. S1 (Supporting Information), the results are listed in Table 1. The decomposition temperatures ( $T_d$  at 5 % weight loss) for **P1–P4** were over 350 °C thus indicating a good thermal stability of these polymers more than sufficient for their application in OSCs. The melting and crystallization peaks were registered for polymers **P1** and **P2**, that might indicate more ordered structure of these compounds in solid state as compared to polymers **P3** and **P4**.

Optical properties of polymers **P1–P4** were investigated in dilute 1,2-dichlorobenzene solutions and in thin films (Fig. 1). The long-wavelength absorption bands (550–760 nm) correspond to HOMO→LUMO transition and are associated with the intramolecular charge transfer in the polymer backbone (see also Fig. 1 and discussion below) [32–34].

The optical spectra of polymer **P3** in solution and thin films are very different because of the remarkable low energy absorption band offset by ~100 nm (Fig. S2). The observed spectacular bathochromic shift while going from the solution to the film suggests that polymer **P3** can undergo efficient supramolecular assembling in solid state [32,35]. At the same time, **P3** chains might undergo most complete disaggregation in solution and have a substantial degree of freedom with respect to backbone tilting and twisting. This is also confirmed by temperature-dependent UV-vis spectra (Fig. S3). Absorption edge in spectra of **P3** is much less affected by the temperature increase from 30 °C to 100 °C as compared to other polymers. Similar though less pronounced effect was also observed for polymer **P1**. In contrast, **P2** and **P4** showed nearly identical spectra in solutions and thin films (Fig. S2). Increase in the temperature of **P2** and **P4** solutions resulted in a pronounced blue-shift of the absorption bands (Fig. S3) thus implying that these polymers undergo a strong aggregation already in solution [36].

The optical band gaps ( $E_g^{\text{opt}}$ ) for polymers **P1–P4** were estimated from the low energy absorption onsets in the spectra of thin films (Table 1). It should be noted that the introduction of additional thiophene spacers into polymer backbones leads to a slight decrease in their band gaps as can be concluded from the comparison of the optical properties of **P3** and **P4** vs. **P1** and **P2**.

Cyclic voltammetry (CV) was employed to investigate the electrochemical behavior of conjugated polymers. The CV curves obtained for thin polymer films are shown in Fig. 1c. Energies of the highest occupied molecular orbital (HOMO) of polymers were estimated considering the onset potentials of the oxidation wave ( $E_{\text{onset}}^{\text{ox}}$ ) and using the value of −5.1 eV as the potential of the  $\text{Fc}^+/\text{Fc}$  redox couple in the Fermi energy scale [37]. The energies of the lowest unoccupied molecular orbital (LUMO) were calculated based on the HOMO and optical band gap values as  $E_{\text{LUMO}} = E_{\text{HOMO}} + E_g^{\text{opt}}$  (Table 1).

Notably, the HOMO/LUMO levels of fluorinated polymers **P2** and **P4** are lying 30–40 meV deeper as compared to that of polymers **P1** and **P3**. Similar electronic effects of the fluorine substitution in conjugated polymers were also reported previously [13,38]. The electron donating effect of thiophene π-bridges on frontier energy levels was found to be much more significant: HOMO levels of **P3** and **P4** are positioned ~200 meV higher than those of polymers **P1** and **P2**.

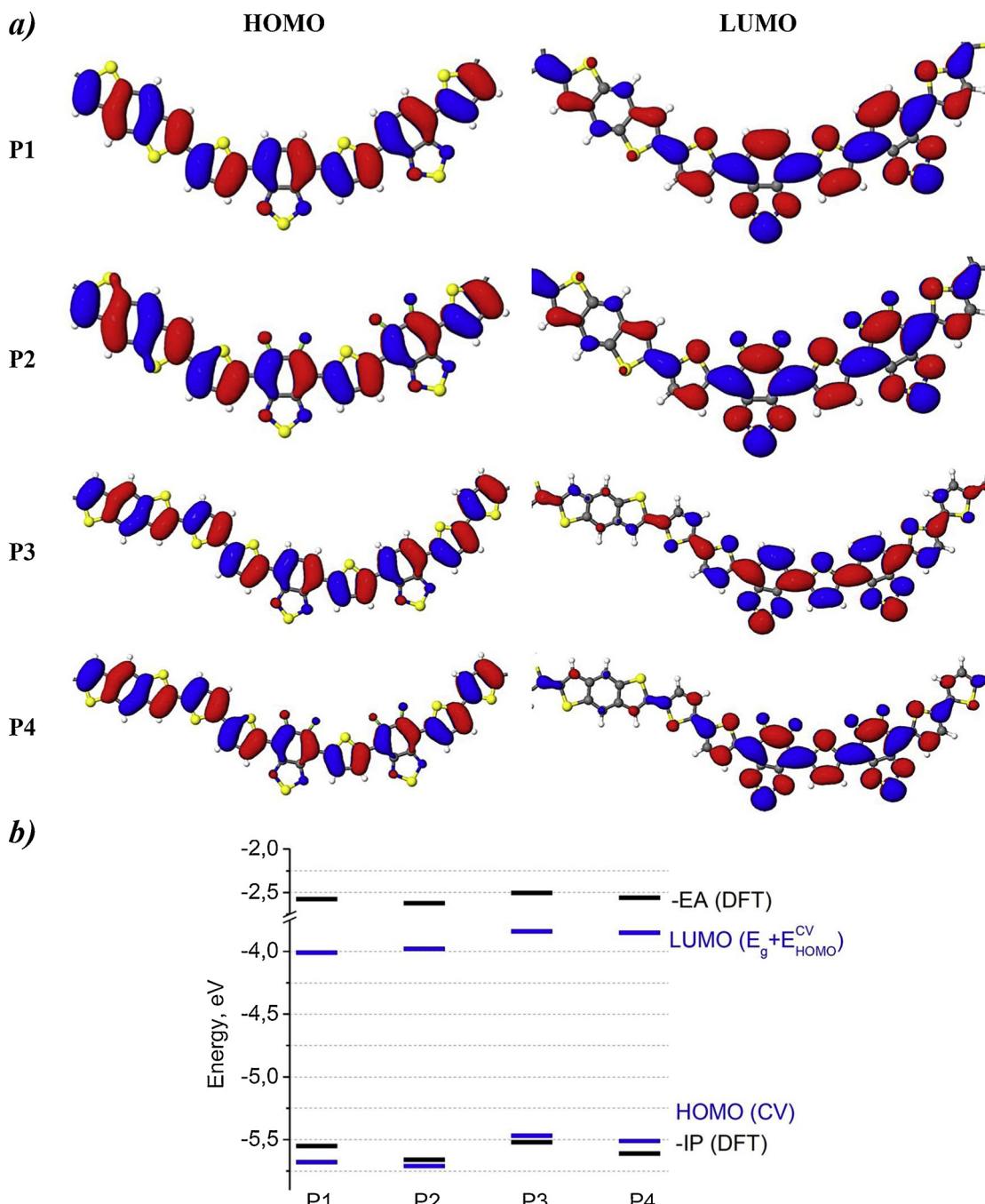


**Fig. 2.** The HOMO and LUMO distribution for polymers **P1-P4** shown for one repeating unit with reduced alkyl chains (a). Frontier molecular orbital energy levels as estimated from CV measurements and predicted by CAM-B3LYP/6-31G\* calculations (b).

**Table 2**

Parameters of OSCs based on the blends of polymers **P1-P4** with [70]PCBM.

Polymer	$V_{OC}$ , mV	$J_{SC}$ , mA/cm <sup>2</sup>	$J_{SC, EQE}$ , mA/cm <sup>2</sup>	FF, %	PCE, %	$\mu_e$ , cm <sup>2</sup> V <sup>-1</sup> s <sup>-1</sup>	$\mu_h$ , cm <sup>2</sup> V <sup>-1</sup> s <sup>-1</sup>
P1	843	8.5	7.3	48	3.4	$4.1 \times 10^{-4}$	$6.0 \times 10^{-4}$
P2	872	3.3	3.9	52	1.5	$2.7 \times 10^{-5}$	$6.3 \times 10^{-5}$
P3	723	9.1	9.9	53	3.5	$9.3 \times 10^{-4}$	$8.0 \times 10^{-4}$
P4	720	15.7	13.6	62	7.0	$9.7 \times 10^{-3}$	$8.1 \times 10^{-3}$

Similar changes associated with the introduction of the thiophene spacer units were also reported earlier [23].

Considering that the achievable open-circuit voltage ( $V_{OC}$ ) of organic solar cells is proportional to the energy offset between the HOMO

of donor and the LUMO of the acceptor, polymers **P1** and **P2** are expected to deliver higher  $V_{OC}$  in organic solar cells as compared to **P3** and **P4**.

Density functional theory (CAM-B3LYP/6-31G\*) calculations were

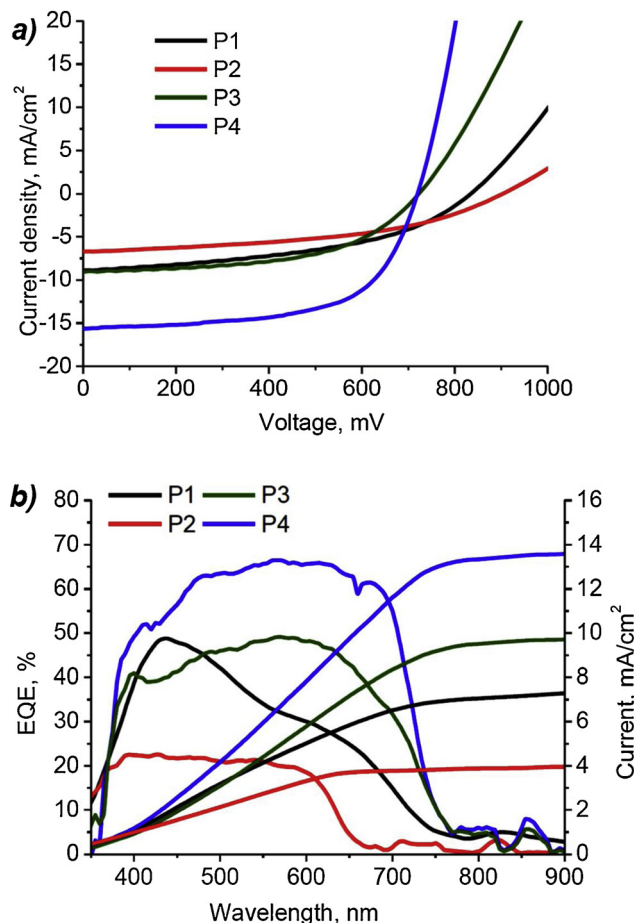


**Fig. 3.** J-V characteristics (a) and EQE (b) spectra of solar cells based on the blends of **P1–P4** with [70]PCBM.

carried out to gain a deeper understanding of the electronic structure and rationalize measured optoelectronic properties of **P1–P4** polymers using the Gaussian 16 program package [39] (see Section S3 for details, Supporting Information). The electron density distributions of HOMO and LUMO are shown in Fig. 2a. As can be seen, the HOMOs of polymers are delocalized along their entire backbones, while the LUMOs are largely localized on the electron withdrawing benzothiadiazole units. The calculated HOMO energy levels (Fig. 2b) agree well with the experimentally measured values (CV) except for a small variation across the set of polymers **P1–P4**, which is mainly because of the accuracy of the used approximation of the idealized polymer model in DFT simulations. At the same time, the typical accuracy of electrochemistry measurements used to probe the oxidation potentials stays within 20–30 meV, which introduces additional uncertainty and possible scattering of the experimental data [40].

Electronic properties of polymers **P1–P4** (Fig. S8) in the ideal planar geometry are very similar: the variation of HOMO/LUMO energies stay within tens of meV (Table S22). The analysis of localized molecular orbitals (LMO) fully explains this picture: all the considered polymers contain the same pairwise interconnections of key building blocks, and thus the variation of LMO energies and inter-block couplings across the set of considered polymers is small (Table S17 and Fig. S7).

Since all the considered polymers are nearly isoelectronic, the experimentally observed large differences in their optoelectronic and photovoltaic (see below) properties might be attributed to the effects of the chain geometry. The set of intramolecular descriptors correlating with the material morphology is a potential energy surface (PES) for flexible dihedrals connecting monomer units into a polymer (Table S18).

Since thiophene is the most flexible unit of a free polymer, **P3** and **P4** structures are more flexible than **P1** and **P2**, which might affect significantly the real nanoscale morphology of the films at the stage of their formation from solution.

Fluorine substitution also substantially changes PES for benzothiadiazole (c.f. columns 'T + B' and 'T + F' in Table S18 where T represents thiophene, B – benzothiadiazole, and F - 5,6-difluorobenzothiadiazole units): while 'T + F' interconnections are planar with 2:1 ratio of rotamer population at the room temperature, 'T + B' connections are nonplanar for the metastable rotamer, and the population ratio is higher, 3:1.

As a consequence, the fluorine-loaded block is more flexible with respect to a 180-degree flip, especially in 'FTF' connections, where the long range electrostatic effects can also play a role. A simplified conformational sampling of **P3** polymer confirms that the observed large absorption shift (~0.5 eV) between solution and thin film is largely due to conformational disorder of the conjugated backbone in the solution (Fig. S13). A part of the shift is probably due to intermolecular delocalization of excitations in thin films [41].

Photovoltaic properties of polymers **P1–P4** were investigated in organic solar cells with the standard configuration: ITO/PEDOT:PSS (60 nm)/active layer (100–180 nm)/Mg (60 nm)/Al (50 nm). The current-voltage characteristics of the devices were measured using the simulated AM1.5 G (100 mW/cm<sup>2</sup>) illumination. Device fabrication conditions were optimized to achieve the best performance of OSCs based on each of the polymers. In particular, the weight ratio of polymer and PCBM and the thickness of blend films were varied. Additionally, we used 1,8-octanedithiol (ODT) as a processing additive and solvent vapor annealing (SVA) technique [42–44] for post-treatment of the deposited blend films. The electrical characteristics of the optimized solar cells are presented in Table 2. The corresponding J-V curves and EQE spectra are shown in Fig. 3. Details on optimization of processing conditions and corresponding photovoltaic parameters of devices are summarized in Tables S1–S15.

The  $J_{SC}$  values obtained from the J-V measurements are in a good agreement with the values estimated by integration of EQE spectra over the reference AM1.5 G solar spectrum. On the one hand, the solar cells based on polymers **P1** and **P2** demonstrated higher open circuit voltages ( $V_{OC}$ ) of 840–870 mV as compared to the devices based on thiophene- $\pi$ -bridged polymers **P3** and **P4** (~720 mV).

This result is fully consistent with the lower HOMO energies of polymers **P1–P2** vs. **P3–P4**. On the other hand, conjugated polymers **P3** and **P4** with additional thiophene fragments provided much higher short-circuit current densities ( $J_{SC}$ ). Interestingly, OSCs based on the fluorine-loaded polymer **P4** showed higher currents than devices based on non-fluorinated **P3**, while for the polymers **P1** and **P2** introduction of fluorine substituents has an opposite effect. The best PCE of 7 % was achieved in solar cells based on polymer **P4**, which could be mainly attributed to the higher  $J_{SC}$  of 15.7 mA/cm<sup>2</sup> and FF of 62 %. It is reasonable to assume that the photovoltaic performance of polymers **P1–P4** is strongly impacted by the charge transport characteristics of the polymer-fullerene blends and their nanoscale morphology. In order to gain a better understanding of these effects, the charge carrier mobilities were estimated for optimized polymer-fullerene blends using the space-charge-limited current (SCLC) technique. To perform the measurements, the hole-only (ITO/PEDOT:PSS(60 nm)/blend/F<sub>4</sub>TTCNQ(1 nm)/MoO<sub>3</sub>(22 nm)/Ag(120 nm)) and the electron-only (ITO/Yb(15 nm)/blend/Ca) devices were fabricated. The thickness of the blend was varied from 100 to 250 nm to reveal realistic mobility values with minimal impact of the interfacial effects induced by the adjacent charge transport layers. The charge carrier mobilities were estimated using a pulsed measurement mode and considering the part of the current-voltage characteristic after the trap filling threshold [45]. It is noteworthy that the blends based on **P3** and **P4** demonstrate higher charge carrier mobilities in comparison with the composite films comprising **P1** or **P2** (Table 2), which might be associated with more planar chain

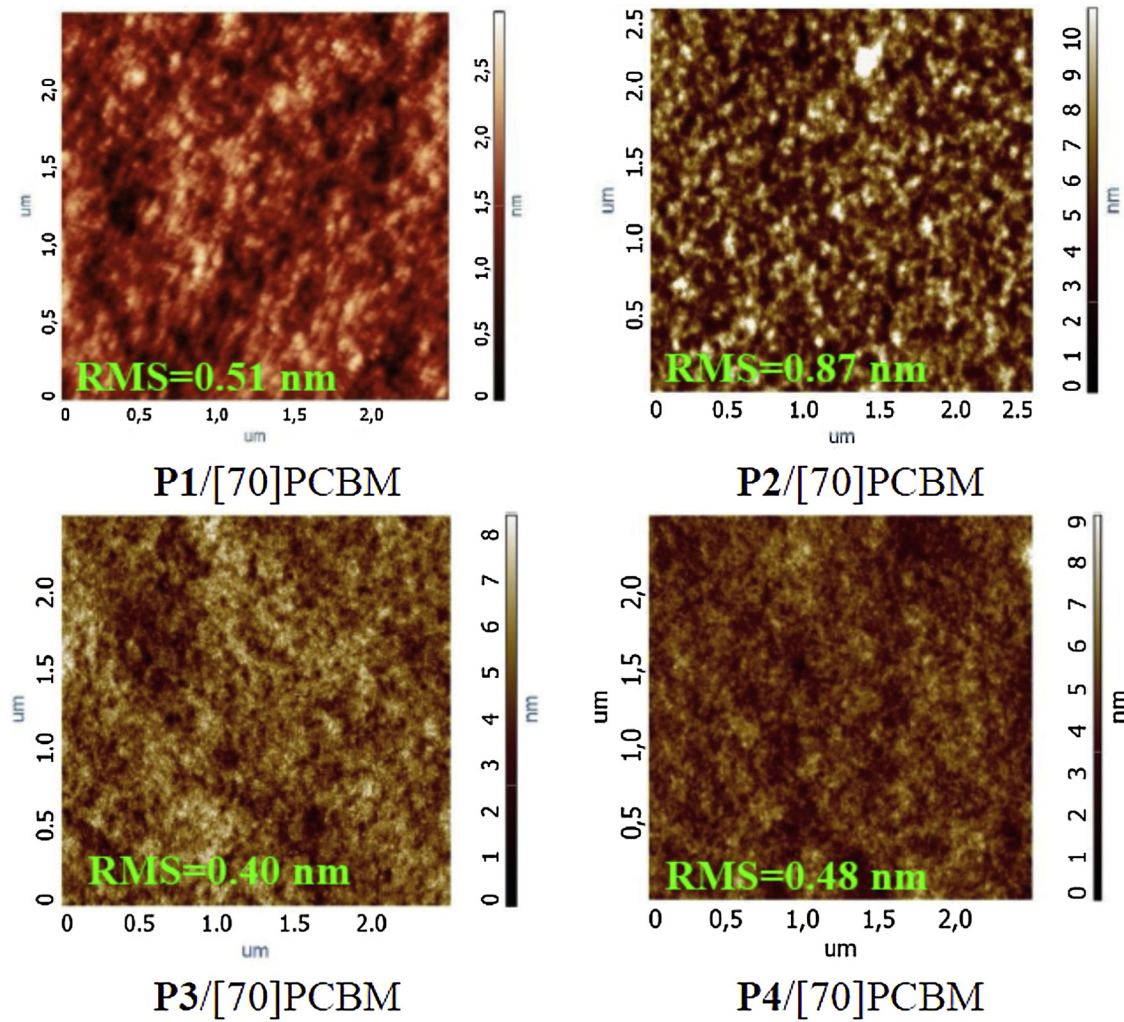


Fig. 4. AFM topography images for thin films of the fullerene-polymer blends.

structures of the thiophene-bridged polymers.

Surprisingly, loading the fluorine into **P1** backbone resulted in a drastic deterioration of hole and electron mobilities in the **P2/[70]PCBM** blend. On the contrary, a shift from non-fluorinated thiophene-bridged polymer **P3** to the fluorine-containing **P4** resulted in a substantial increase in charge carrier mobilities in polymer-fullerene blends. This phenomenon might be explained by different morphology of the blend films as described below. The highest mobilities of  $9.7 \times 10^{-3} \text{ cm}^2 \text{V}^{-1} \text{s}^{-1}$  and more balanced  $\mu_h/\mu_e$  ratio of 0.84 were achieved for the **P4/[70]PCBM**, which is consistent with the best photovoltaic performance of this system. On the contrary, the worst performing in solar cells system **P2/[70]PCBM** is also characterized by the lowest and unbalanced mobilities of holes and electrons ( $\mu_h/\mu_e > 2$ ). Thus, there is a clear correlation between the photovoltaic performance of the fullerene-polymer blends and their transport characteristics.

Other important features affecting the performance of organic solar cells might be the microstructural parameters of conjugated polymers and nanoscale morphology of the active layer. We assessed crystallinity of polymers using X-ray diffraction (XRD, Fig. S4) [46–48], while the surface topography of the polymer-fullerene blends was studied using atomic force microscopy (AFM, Fig. 4). All polymers are amorphous according to powder XRD results, with XRD patterns displaying the typical wide amorphous halos at high  $2\theta$  angles of 15–35 deg. The worst-performing **P2/[70]PCBM** system showed clear signatures of a large-scale phase separation as can be concluded from the appearance

of large grains approaching 200–300 nm in size. Moreover, the highest root-mean-square (RMS) roughness of 0.87 nm for **P2/[70]PCBM** was observed. Such morphology and high RMS implies inhomogeneous distribution of the fullerene and polymer phases in the films due to their poor miscibility. Considering short exciton diffusion lengths in organic semiconductors, so large phase segregation is not favorable for efficient exciton dissociation [49,50] resulting in their massive recombination and hence low  $J_{SC}$  values. Similar effects were generally observed for multiple fullerene-polymer blends [51–53]. Interestingly, polymer **P1** forms much more homogeneous blends with [70]PCBM as compared to **P2** (RMS = 0.51 nm), therefore poor compatibility of the components is induced by the introduction of fluorine substituents in benzothiadiazole acceptor units. On the contrary, both **P3/[70]PCBM** and **P4/[70]PCBM** blends displayed uniform and well-organized film structure with no signs of large-scale phase segregation between the conjugated polymers and [70]PCBM. RMS values for **P3/[70]PCBM** and **P4/[70]PCBM** blend films were 0.40 nm and 0.48 nm, respectively, thus indicating better miscibility of these polymers with the acceptor component.

This observation suggests that insertion of thiophene  $\pi$ -bridges in the polymer structure improves miscibility of the blend components presumably owing to charge transfer interactions of the electron rich thiophene units and electron deficient fullerene cages. [54] Optimal blend morphology enables significantly improved current densities in solar cells based on the polymers **P3** and **P4** as compared to the devices comprised of **P1** and **P2** blends with [70]PCBM.

### 3. Conclusion

We synthesized and investigated four novel conjugated polymers based on benzodithiophene, thiophene and 2,1,3-benzothiadiazole or 5,6-difluoro-2,1,3-benzothiadiazole. The effects of fluorine substitution and introduction of  $\pi$ -spacer on the optoelectronic properties, charge carriers mobility, blend morphology, and photovoltaic performance were revealed. While comparing the photovoltaic characteristics of polymers **P1** and **P2**, one can conclude that incorporation of fluorine substituents into polymer structure without thiophene  $\pi$ -bridge results in a significant deterioration of charge carrier mobilities caused by large-scale phase separation of the fullerene and polymer components in the active layer. Thus, loading the polymer with fluorine changes its surface energy and reduces its miscibility with the fullerene acceptor. Comparing polymers **P1** and **P3** suggests that introduction of thiophene  $\pi$ -spacers does not improve photovoltaic performance of the material presumably due to a voltage loss (because of higher HOMO energy of **P3**) and still unbalanced blend morphology. However, a combination of the two aforementioned approaches was shown to be a promising strategy for improving the charge carrier mobilities and nanoscale morphology of polymer-fullerene blends leading to twice higher power conversion efficiencies (PCE ~ 7 %) achieved in solar cells based on polymer **P4** in comparison with the reference devices based on **P1**. The presented here results for the model (X-DADAD)<sub>n</sub>-type conjugated polymers pave a way to further rational design of new materials for efficient and stable organic solar cells.

### Declaration of Competing Interest

The authors declare that they have no known competing financial interests or personal relationships that could have appeared to influence the work reported in this paper.

### Acknowledgement

This work was funded by the Russian Science Foundation (grant No. 18-13-00205).

### Appendix A. Supplementary data

Supplementary material related to this article can be found, in the online version, at doi:<https://doi.org/10.1016/j.synthmet.2019.116231>.

### References

- [1] Y. Li, G. Xu, C. Cui, Y. Li, Flexible and semitransparent organic solar cells, *Adv. Energy Mater.* 8 (2018) 1701791, , <https://doi.org/10.1002/aenm.201701791>.
- [2] W. Zhao, S. Li, H. Yao, S. Zhang, Y. Zhang, B. Yang, J. Hou, Molecular optimization enables over 13% efficiency in organic solar cells, *J. Am. Chem. Soc.* 139 (2017) 7148–7151, <https://doi.org/10.1021/jacs.7b02677>.
- [3] W. Wang, B. Zhao, Z. Cong, Y. Xie, H. Wu, Q. Liang, S. Liu, F. Liu, C. Gao, H. Wu, Y. Cao, Nonfullerene polymer solar cells based on a main-chain twisted low-bandgap acceptor with power conversion efficiency of 13.2%, *ACS Energy Lett.* 3 (2018) 1499–1507, <https://doi.org/10.1021/acsenergylett.8b00627>.
- [4] X. Zhang, D. Zhang, Q. Zhou, R. Wang, J. Zhou, J. Wang, H. Zhou, Y. Zhang, Fluorination with an enlarged dielectric constant prompts charge separation and reduces bimolecular recombination in non-fullerene organic solar cells with a high fill factor and efficiency & 13%, *Nano Energy* 56 (2019) 494–501, <https://doi.org/10.1016/j.nanoen.2018.11.067>.
- [5] W. Gao, T. Liu, Z. Luo, L. Zhang, R. Ming, C. Zhong, W. Ma, H. Yan, C. Yang, Regulating exciton bonding energy and bulk heterojunction morphology in organic solar cells via methyl-functionalized non-fullerene acceptors, *J. Mater. Chem. A* 7 (2019) 6809–6817, <https://doi.org/10.1039/C9TA00597H>.
- [6] Y. Cui, H. Yao, L. Hong, T. Zhang, Y. Xu, K. Xian, B. Gao, J. Qin, J. Zhang, Z. Wei, J. Hou, Achieving over 15% efficiency in organic photovoltaic cells via copolymer design, *Adv. Mater.* 31 (2019) 1808356, , <https://doi.org/10.1002/adma.201808356>.
- [7] R. Peng, H. Guo, J. Xiao, G. Wang, S. Tan, B. Zhao, X. Guo, Y. Li, Synergistic effect of fluorine substitution and thio-alkylation on photovoltaic performances of alternating conjugated polymers based on alkylthio-substituted benzothiadiazole-, quaterthiophene, *ACS Appl. Energy Mater.* 1 (2018) 2192–2199, <https://doi.org/10.1021/acsaeam.8b00238>.
- [8] S. Furukawa, H. Komiyama, T. Yasuda, Controlling open-circuit voltage in organic solar cells by terminal fluoro-functionalization of narrow-bandgap  $\pi$ -conjugated molecules, *J. Phys. Chem. C* 120 (2016) 21235–21241, <https://doi.org/10.1021/acs.jpcc.6b06758>.
- [9] M.L. Keshtov, S.A. Kuklin, A.R. Khokhlov, I.O. Konstantinov, N.V. Nekrasova, Z. Xie, S. Biswas, G.D. Sharma, Polymer solar cells based on D-A low bandgap copolymers containing fluorinated side chains of thiadiazoloquinoxaline acceptor and benzodithiophene donor units, *New J. Chem.* 42 (2018) 1626–1633, <https://doi.org/10.1039/C7NJ03981F>.
- [10] S. Song, S. Kim, W. Kim, S.S. Park, S.H. Park, Y. Jin, Synthesis and photovoltaic properties of copolymers with a fluoro quinoxaline unit, *J. Polym. Sci. Part A: Polym. Chem.* 56 (2018) 821–830, <https://doi.org/10.1002/pola.28957>.
- [11] P. Shen, H. Bin, Y. Zhang, Y. Li, Synthesis and optoelectronic properties of new D-A copolymers based on fluorinated benzothiadiazole and benzoselenadiazole, *Polym. Chem.* 5 (2014) 567–577, <https://doi.org/10.1039/C3PY00968H>.
- [12] G. Liu, C. Wang, P. Yin, S. Tan, P. Shen, Impact of the number of fluorine atoms on crystalline, physicochemical and photovoltaic properties of low bandgap copolymers based on 1,4-dithienylphenylene and diketopyrrolopyrrole, *Polymer* 125 (2017) 217–226, <https://doi.org/10.1016/J.POLYMER.2017.08.018>.
- [13] N. Leclerc, P. Chávez, O. Ibraikulov, T. Heiser, P. Lévéque, Impact of backbone fluorination on  $\pi$ -conjugated polymers in organic photovoltaic devices: a review, *Polymers* 8 (2016) 11, <https://doi.org/10.3390/polym8010011>.
- [14] H. Zhou, L. Yang, A.C. Stuart, S.C. Price, S. Liu, W. You, Development of fluorinated benzothiadiazole as a structural unit for a polymer solar cell of 7 % efficiency, *Angew. Chemie Int. Ed.* 50 (2011) 2995–2998, <https://doi.org/10.1002/anie.201005451>.
- [15] N. Wang, Z. Chen, W. Wei, Z. Jiang, Fluorinated benzothiadiazole-based conjugated polymers for high-performance polymer solar cells without any processing additives or post-treatments, *J. Am. Chem. Soc.* 135 (2013) 17060–17068, <https://doi.org/10.1021/ja409881g>.
- [16] P. Zhou, D. Dang, J. Fan, W. Xiong, C. Yang, H. Tan, Y. Wang, Y. Liu, W. Zhu, Increasing thiophene spacers between thieno[3,2-b]thiophene and benzothiadiazole units in backbone to enhance photovoltaic performance for their 2-D polymers, *Dyes Pigm.* 112 (2015) 99–104, <https://doi.org/10.1016/j.dyepig.2014.06.015>.
- [17] S. Liu, X. Bao, W. Li, K. Wu, G. Xie, R. Yang, C. Yang, Benzo[1,2-b:4,5-b']dithiophene and thieno[3,4-c]pyrrole-4,6-dione based Donor- $\pi$ -acceptor conjugated polymers for high performance solar cells by rational structure modulation, *Macromolecules* 48 (2015) 2948–2957, <https://doi.org/10.1021/acs.macromol.5b00251>.
- [18] H. Zheng, J. Wang, W. Chen, C. Gu, J. Ren, M. Qiu, R. Yang, M. Sun, Efficiency enhancement in an indacenodithiophene and thieno[3,4-c]pyrrole-4,6-dione backbone photovoltaic polymer with an extended thieno[3,2-b]thiophene  $\pi$ -bridge, *J. Mater. Chem. C* 4 (2016) 6280–6286, <https://doi.org/10.1039/C6TC01238H>.
- [19] X. Gao, Y. Li, L. Yu, F. Hou, T. Zhu, X. Bao, F. Li, M. Sun, R. Yang, The regulation of  $\pi$ -bridge of indacenodithiophene-based donor- $\pi$ -acceptor conjugated polymers toward efficient polymer solar cells, *Dyes Pigm.* 162 (2019) 43–51, <https://doi.org/10.1016/J.DYEPIG.2018.10.008>.
- [20] T. Zhu, Y. Zhang, Y. Li, X. Song, Z. Liu, S. Wen, X. Bao, M. Sun, R. Yang, Acceptor-rich bulk heterojunction polymer solar cells with balanced charge mobilities, *Org. Electron.* 51 (2017) 16–24, <https://doi.org/10.1016/J.ORGEL.2017.08.031>.
- [21] J. Ren, X. Bao, L. Han, J. Wang, M. Qiu, Q. Zhu, T. Hu, R. Sheng, M. Sun, R. Yang, 4,7-Di-2-thienyl-2,1,3-benzothiadiazole with hexylthiophene side chains and a benzodithiophene based copolymer for efficient organic solar cells, *Polym. Chem.* 6 (2015) 4415–4423, <https://doi.org/10.1039/C5PY00199D>.
- [22] H. Bin, L. Xiao, Y. Liu, P. Shen, Y. Li, Effects of donor unit and  $\pi$ -bridge on photovoltaic properties of D-A copolymers based on benzo[1,2-b:4,5-c']dithiophene-4,8-dione acceptor unit, *J. Polym. Sci. Part A: Polym. Chem.* 52 (2014) 1929–1940, <https://doi.org/10.1002/pola.27209>.
- [23] X. Wang, Y. Sun, S. Chen, X. Guo, M. Zhang, X. Li, Y. Li, H. Wang, Effects of  $\pi$ -Conjugated bridges on photovoltaic properties of donor- $\pi$ -acceptor conjugated copolymers, *Macromolecules* 45 (2012) 1208–1216, <https://doi.org/10.1021/ma202656b>.
- [24] A.V. Akkuratov, D.K. Susarova, O.V. Kozlov, A.V. Chernyak, Y.L. Moskvin, L.A. Frolova, M.S. Pshenichnikov, P.A. Troshin, Design of (X-DADAD)<sub>n</sub> type copolymers for efficient bulk heterojunction organic solar cells, *Macromolecules* 48 (2015) 2013–2021, <https://doi.org/10.1021/ma5023956>.
- [25] L.A. Frolova, N.P. Piven, D.K. Susarova, A.V. Akkuratov, S.D. Babenko, P.A. Troshin, ESR spectroscopy for monitoring the photochemical and thermal degradation of conjugated polymers used as electron donor materials in organic bulk heterojunction solar cells, *Chem. Commun.* 51 (2015) 2242–2244, <https://doi.org/10.1039/C4CC01846C>.
- [26] W.R. Mateker, I.T. Sachs-Quintana, G.F. Burkhard, R. Cheacharoen, M.D. McGehee, Minimal long-term intrinsic degradation observed in a polymer solar cell illuminated in an oxygen-free environment, *Chem. Mater.* 27 (2015) 404–407, <https://doi.org/10.1021/cm504650a>.
- [27] M.C. Scharber, On the efficiency limit of conjugated polymer: fullerene-based bulk heterojunction solar cells, *Adv. Mater.* 28 (2016) 1994–2001, <https://doi.org/10.1002/adma.201504914>.
- [28] A.V. Akkuratov, D.K. Susarova, L.N. Inasaridze, P.A. Troshin, The effect of the fluorine loading on the optoelectronic and photovoltaic properties of (X-DADAD)<sub>n</sub>-type donor-acceptor copolymers with the benzothiadiazole A units, *Phys. Status Solidi - Rapid Res. Lett.* 11 (2017) 1700087, , <https://doi.org/10.1002/pssr.201700087>.
- [29] A.V. Akkuratov, D.K. Susarova, Y.L. Moskvin, D.V. Anokhin, A.V. Chernyak,

- F.A. Prudnov, D.V. Novikov, S.D. Babenko, P.A. Troshin, A strong influence of the positions of solubilizing alkyl side chains on optoelectronic and photovoltaic properties of TTBTBTT-based conjugated polymers, *J. Mater. Chem. C* 3 (2015) 1497–1506, <https://doi.org/10.1039/C4TC02432J>.
- [30] M. Wang, X. Hu, P. Liu, W. Li, X. Gong, F. Huang, Y. Cao, Donor–acceptor conjugated polymer based on naphtho[1,2-c:5,6-c]bis[1,2,5]thiadiazole for high-performance polymer solar cells, *J. Am. Chem. Soc.* 133 (2011) 9638–9641, <https://doi.org/10.1021/ja201131h>.
- [31] A.V. Akkuratov, F.A. Prudnov, L.N. Inasaridze, P.A. Troshin, Synthesis of the (X-DADAD) n-type conjugated polymers with 2,1,3-benzoxadiazole acceptor blocks and their application in organic solar cells, *Tetrahedron Lett.* 58 (2017) 97–100, <https://doi.org/10.1016/j.tetlet.2016.11.107>.
- [32] J. Lu, Y. Yao, P.M. Shenai, L. Chen, Y. Zhao, Elucidating the enhancement in optical properties of low band gap polymers by tuning the structure of alkyl side chains, *Phys. Chem. Chem. Phys.* 17 (2015) 9541–9551, <https://doi.org/10.1039/C4CP05657D>.
- [33] D. Chen, Y. Zhao, C. Zhong, G. Yu, Y. Liu, J. Qin, A structurally ordered thiophene-thiazole copolymer for organic thin-film transistors, *Sci. China Chem.* 55 (2012) 760–765, <https://doi.org/10.1007/s11426-011-4460-2>.
- [34] Y. Zhu, R.D. Champion, S.A. Jenekhe, Conjugated donor–acceptor copolymer semiconductors with large intramolecular charge transfer: synthesis, optical properties, electrochemistry, and field effect carrier mobility of thienopyrazine-based copolymers, *Macromolecules* 39 (2006) 8712–8719, <https://doi.org/10.1021/ma061861g>.
- [35] P.J. Brown, D.S. Thomas, A. Köhler, J.S. Wilson, J.-S. Kim, C.M. Ramsdale, H. Sirringhaus, R.H. Friend, Effect of interchain interactions on the absorption and emission of poly(3-hexylthiophene), *Phys. Rev. B* 67 (2003) 064203, , <https://doi.org/10.1103/PhysRevB.67.064203>.
- [36] Y. Zou, A. Najari, P. Berrouard, S. Beaupré, B. Réda Aich, Y. Tao, M. Leclerc, A thieno[3,4-c]pyrrole-4,6-dione-based copolymer for efficient solar cells, *J. Am. Chem. Soc.* 132 (2010) 5330–5331, <https://doi.org/10.1021/ja101888b>.
- [37] C.M. Cardona, W. Li, A.E. Kaifer, D. Stockdale, G.C. Bazan, Electrochemical considerations for determining absolute frontier orbital energy levels of conjugated polymers for solar cell applications, *Adv. Mater.* 23 (2011) 2367–2371, <https://doi.org/10.1002/adma.201004554>.
- [38] Q. Zhang, M.A. Kelly, N. Bauer, W. You, The curious case of fluorination of conjugated polymers for solar cells, *Acc. Chem. Res.* 50 (2017) 2401–2409, <https://doi.org/10.1021/acs.accounts.7b00326>.
- [39] M.J. Frisch, G.W. Trucks, H.B. Schlegel, G.E. Scuseria, M.A. Robb, J.R. Cheeseman, G. Scalmani, V. Barone, G.A. Petersson, H. Nakatsuji, X. Li, M. Caricato, A. Marenich, J. Bloino, B.G. Janesko, R. Gomperts, B. Mennucci, H.P. Hratchian, J.V. Ortiz, A.F. Izmaylov, J.L. Sonnenberg, D. Williams-Young, F. Ding, F. Lipparini, F. Egidi, J. Goings, B. Peng, A. Petrone, T. Henderson, D. Ranasinghe, V.G. Zakrzewski, J. Gao, N. Rega, G. Zheng, W. Liang, M. Hada, M. Ehara, K. Toyota, R. Fukuda, J. Hasegawa, M. Ishida, T. Nakajima, Y. Honda, O. Kitao, H. Nakai, T. Vreven, K. Throssell, J.A.J. Montgomery, J.E. Peralta, F. Ogliaro, M. Bearpark, J.J. Heyd, E. Brothers, K.N. Kudin, V.N. Staroverov, T. Keith, R. Kobayashi, J. Normand, K. Raghavachari, A. Rendell, J.C. Burant, S.S. Iyengar, J. Tomasi, M. Cossi, J.M. Millam, M.A. Klene, C.R. Cammi, J.W.M. Ochterski, R.L. Morokuma, K.O. Farkas, J.B. Foresman, D.J. Fox, Gaussian 09, Revision A.02, Gaussian, Inc., Wallingford CT, 2016.
- [40] B.M. Savoie, N.E. Jackson, T.J. Marks, M.A. Ratner, Reassessing the use of one-electron energetics in the design and characterization of organic photovoltaics, *Phys. Chem. Chem. Phys.* 15 (2013) 4538–4547, <https://doi.org/10.1039/c3cp50438g>.
- [41] N.J. Hestand, F.C. Spano, Expanded theory of H- and J-molecular aggregates: the effects of vibronic coupling and intermolecular charge transfer, *Chem. Rev.* 118 (2018) 7069–7163, <https://doi.org/10.1021/acs.chemrev.7b00581>.
- [42] C.D. Wessendorf, J. Hanisch, E. Ahlsweide, A. Perez-Rodriguez, E. Barrena, A.P. Arndt, U. Lemmer, I. Ata, G.L. Schulz, P. Bäuerle, A. Quintilla, P. Wochner, Understanding the effect of solvent vapor annealing on solution-processed A-D-A oligothiophene bulk-heterojunction solar cells: the role of alkyl side chains, *J. Mater. Chem. A* 4 (2016) 2571–2580, <https://doi.org/10.1039/C5TA07713C>.
- [43] S. Engmann, H.W. Ro, A. Herzing, C.R. Snyder, L.J. Richter, P.B. Geraghty, D.J. Jones, Film morphology evolution during solvent vapor annealing of highly efficient small molecule donor/acceptor blends, *J. Mater. Chem. A* 4 (2016) 15511–15521, <https://doi.org/10.1039/C6TA05056E>.
- [44] J. Min, N.S. Güldal, J. Guo, C. Fang, X. Jiao, H. Hu, T. Heumüller, H. Ade, C.J. Brabec, Gaining further insight into the effects of thermal annealing and solvent vapor annealing on time morphological development and degradation in small molecule solar cells, *J. Mater. Chem. A* 5 (2017) 18101–18110, <https://doi.org/10.1039/C7TA04769J>.
- [45] V. Podzorov, S.E. Sysoev, E. Loginova, V.M. Pudalov, M.E. Gershenson, Single-crystal organic field effect transistors with the hole mobility ~8 cm<sup>2</sup>/Vs, *Appl. Phys. Lett.* 83 (2003) 3504–3506, <https://doi.org/10.1063/1.1622799>.
- [46] S.J. Jeon, S.J. Nam, Y.W. Han, T.H. Lee, D.K. Moon, Molecular design through computational simulation on the benzo[2,1-b;3,4-b]dithiophene-based highly ordered donor material for efficient polymer solar cells, *Polym. Chem.* 8 (2017) 2979–2989, <https://doi.org/10.1039/c7py00292k>.
- [47] S.J. Jeon, J.E. Yu, Y.W. Han, I.S. Suh, D.K. Moon, Structural optimization in the same polymer backbones for efficient polymer solar cells: relationship between steric hindrance and molecular weight, *J. Ind. Eng. Chem.* 71 (2019) 137–149, <https://doi.org/10.1016/j.jiec.2018.11.016>.
- [48] S.J. Jeon, Y.W. Han, D.K. Moon, 13.9%-efficiency and eco-friendly nonfullerene polymer solar cells obtained by balancing molecular weight and solubility in chlorinated thiophene-based polymer backbones, *Small* 15 (2019) 1902598, , <https://doi.org/10.1002/smll.201902598>.
- [49] D.E. Markov, C. Tanase, P.W.M. Blom, J. Wildeman, Simultaneous enhancement of charge transport and exciton diffusion in poly(p-phenylene vinylene) derivatives, *Phys. Rev. B* 72 (2005) 045217, , <https://doi.org/10.1103/PhysRevB.72.045217>.
- [50] D.E. Markov, E. Amsterdam, P.W.M. Blom, A.B. Sieval, J.C. Hummelen, Accurate measurement of the exciton diffusion length in a conjugated polymer using a heterostructure with a side-chain cross-linked fullerene layer, *J. Phys. Chem. A* 109 (2005) 5266–5274, <https://doi.org/10.1021/jp0509663>.
- [51] P.A. Troshin, D.K. Susharova, E.A. Khakina, A.A. Goryachev, O.V. Borshchev, S.A. Ponomarenko, V.F. Razumov, N.S. Sariciftci, Material solubility and molecular compatibility effects in the design of fullerene/polymer composites for organic bulk heterojunction solar cells, *J. Mater. Chem.* 22 (2012) 18433–18441, <https://doi.org/10.1039/c2jm32873a>.
- [52] J.A. Renz, P.A. Troshin, G. Gobsch, V.F. Razumov, H. Hoppe, Fullerene solubility-current density relationship in polymer solar cells, *Phys. Status Solidi - Rapid Res. Lett.* 2 (2008) 263–265, <https://doi.org/10.1002/pssr.200802199>.
- [53] P.A. Troshin, H. Hoppe, J. Renz, M. Egginger, J.Y. Mayorova, A.E. Goryachev, A.S. Peregovud, R.N. Lyubovskaya, G. Gobsch, N.S. Sariciftci, V.F. Razumov, Material solubility-photovoltaic performance relationship in the design of novel fullerene derivatives for bulk heterojunction solar cells, *Adv. Funct. Mater.* 19 (2009) 779–788, <https://doi.org/10.1002/adfm.200801189>.
- [54] P.A. Troshin, E.A. Khakina, M. Egginger, A.E. Goryachev, S.I. Troyanov, A. Fuchsbauer, A.S. Peregovud, R.N. Lyubovskaya, V.F. Razumov, N.S. Sariciftci, Self-assembly of thiophene- and furan-appended methanofullerenes with poly(3-hexylthiophene) in organic solar cells, *ChemSusChem* 3 (2010) 356–366, <https://doi.org/10.1002/cssc.200900196>.

## Supporting Information

### Effects of $\pi$ -spacer and fluorine loading on the optoelectronic and photovoltaic properties of $(X\text{-DADAD})_n$ benzodithiophene-based conjugated polymers

Alexander V. Akkuratov,\* Ilya E. Kuznetsov, Petr M. Kuznetsov, Nikita V. Tukachev, Ilya V. Martynov, Sergey L. Nikitenko, Artyom V. Novikov, Alexander V. Chernyak, Andriy Zhugayevych and Pavel A. Troshin

#### Materials and instrumentation

All solvents and reagents were purchased from Sigma-Aldrich or Acros Organics and used as received or purified according to standard procedures. Compounds (4,8-bis(4,5-didecylthiophen-2-yl)benzo[1,2-b:4,5-b']dithiophene-2,6-diyl)bis(trimethylstannane) (**D1**) [1], **M1** [2] and **M4** [3] were synthesized according to the previously reported methods.

Absorption spectra were measured on Avantes AvaSpec-2048 optical fiber spectrometer. The optical spectra of thin films were recorded using 2-channel AvaSpec-2048-2 optical fiber spectrometer integrated inside the glove box. The  $^1\text{H}$  and  $^{13}\text{C}$  NMR spectra were obtained using Bruker AVANCE 600 instrument.

AFM images were obtained using a NTEGRA PRIMA instrument (NT-MDT, Russia).

Cyclic voltammetry measurements were performed for thin films (150–250 nm) of polymers **P1-P4** deposited on a glassy carbon disc electrode following the previously reported procedure [4].

Organic bulk heterojunction solar cells were fabricated using the composites of conjugated polymers **P1-P4** (7 mg) with [60]PCBM or [70]PCBM (7±21 mg) following a general procedure reported previously [4]. Active area of devices was 30 mm<sup>2</sup>.

Thermal (TGA and DSC) measurements were carried out on METTLER TOLEDO TGA/DSC 3+ instrument (Mettler-Toledo AG, Analytical, Switzerland) under nitrogen flow with a heating rate of 15°C min<sup>-1</sup>.

X-ray diffraction analysis was performed using Bruker D8 Advance X-Ray diffractometer with CuK $\alpha$  radiation and LYNXEYE XY Detector in the 2 $\theta$  range 5–45°.

#### Synthesis of compound **1a**

Compound **M1** (1.0 g, 0.89 mmol) and tributyl(thiophen-2-yl)stannane (0.665 g, 1.78 mmol) were placed under argon in a two-necked flask equipped with a reflux condenser. Then toluene (50 mL) and tetrakis(triphenylphosphine)palladium(0) (10 mg) were added. The mixture was heated at reflux within 24h, then cooled down to the room temperature and poured into methanol. The formed precipitate was collected by filtration and washed with methanol. The yield of the dark purple crystalline powder of **1a** was 96%.  $^1\text{H}$  NMR ( $\text{CDCl}_3$ , 600 MHz,  $\delta$ ): 8.25 (s, 2H), 8.02 (s, 2H), 7.99 (d,  $J=7.63$  Hz, 2H), 7.90 (d,  $J=7.63$  Hz, 2H), 7.38 (d,  $J=5.12$  Hz, 2H), 7.27 (d,  $J=3.51$  Hz, 2H), 7.14 (t,  $J=3.61$  Hz, 2H), 2.81 (d,  $J=7.33$  Hz, 4H), 1.83 (m, 2H), 1.27 (m, 48H), 0.90 (t,  $J=7.03$  Hz, 12H) ppm.  $^{13}\text{C}$  NMR ( $\text{CDCl}_3$ , 126 MHz,  $\delta$ ): 152.67, 152.63, 140.60, 139.90, 136.78, 136.03, 133.09, 131.35, 128.48, 127.45, 126.49, 125.95, 125.74, 125.20, 38.84, 34.18, 33.94, 33.49, 33.44, 31.96, 30.09, 29.67, 29.39, 29.27, 29.15, 26.47, 26.46, 24.94, 22.73, 14.15 ppm.

### *Synthesis of compound 1b*

Compound **1b** was prepared following the procedure given for compound **1a** using compound **M2** (1 g, 0.84 mmol) and tributyl(thiophen-2-yl)stannane (0.624 g, 1.67 mmol). The yield of **1b** was 94%. <sup>1</sup>H NMR (CDCl<sub>3</sub>, 600 MHz, δ): 8.25 (s, 2H), 8.00 (s, 2H), 7.36 (d, J=5.12 Hz, 2H), 7.21 (d, J=3.51 Hz, 2H), 7.10 (dd, J=1.61 Hz, J=3.61Hz, 2H), 2.72 (d, J=7.23 Hz, 4H), 1.77 (m, 2H), 1.28 (m, 48H), 0.91 (m, 12H) ppm. <sup>13</sup>C NMR (CDCl<sub>3</sub>, 126 MHz, δ): 151.13, 150.66, 149.22, 148.65, 148.44, 138.88, 135.55, 135.40, 134.61, 130.68, 129.15, 127.44, 126.54, 125.92, 111.65, 110.71, 38.70, 33.72, 33.99, 31.97, 30.12, 29.79, 29.70, 29.42, 26.44, 22.75, 14.15 ppm

### *Synthesis of compound M3*

Compound **1a** (1 g, 0.88 mmol) was dissolved in 20 mL of 1,2-dichlorobenzene and *N*-bromosuccinimide (0.315 g, 1.77 mmol) was added in small portions. The mixture was stirred at room temperature for 60 min, then the solvent was evaporated and the product was washed with ethanol and acetone. Yield =98%. <sup>1</sup>H NMR (CDCl<sub>3</sub>, 600 MHz, δ): 8.26 (s, 2H), 8.02 (s, 2H), 7.99 (d, J=5.71 Hz, 2H), 7.90 (d, J=7.65 Hz, 2H), 7.08 (d, J=3.77 Hz, 2H), 7.02 (d, J=3.77 Hz, 2H), 2.77 (d, J=7.14 Hz, 4H), 1.81 (m, 2H), 1.28 (m, 48H), 0.90 (m, 12H) ppm. <sup>13</sup>C NMR (CDCl<sub>3</sub>, 126 MHz, δ): 152.65, 140.42, 137.56, 137.31, 132.01, 131.13, 130.29, 129.89, 129.16, 126.70, 125.74, 125.34, 124.05, 38.92, 34.18, 31.95, 30.07, 29.72, 29.68, 29.38, 29.26, 29.15, 26.50, 26.48, 24.94, 22.73, 22.71, 14.16, 14.14 ppm.

### *Synthesis of compound M4*

Compound **M4** was synthesized following the procedure given for compound **M3** using **1b** (1 g, 0.83 mmol) and *N*-bromosuccinimide (0.296 g, 1.66 mmol). Yield =96%. <sup>1</sup>H NMR (CDCl<sub>3</sub>, 600 MHz, δ): 8.02 (s, 2H), 7.80 (s, 2H), 6.96 (d, J=3.71 Hz, 2H), 6.85 (d, J=3.71 Hz, 2H), 2.57 (d, J=7.23 Hz, 4H), 1.69 (m, 2H), 1.30 (m, 48H), 0.92 (m, 12H) ppm. <sup>13</sup>C NMR (CDCl<sub>3</sub>, 126 MHz, δ): 148.94, 148.56, 148.31, 148.22, 138.98, 137.08, 134.74, 134.33, 134.25, 130.18, 129.37, 126.36, 112.50, 111.12, 110.51, 38.62, 33.69, 33.37, 32.07, 29.83, 29.75, 29.46, 26.43, 26.39, 22.79, 22.74, 14.27, 14.24, 14.17 ppm.

### *Synthesis of polymers P1-P4*

Polymers **P1-P4** were synthesized and purified following the general procedure reported previously [5].

#### **Polymer P1**

Polymer **P1** was synthesized using monomers **M1** (0.225 g, 0.2 mmol) and **D1** (0.248 g, 0.2 mmol). Yield – 82%. M<sub>w</sub>= 152 kDa, M<sub>w</sub>/M<sub>n</sub>=1.6

#### **Polymer P2**

Polymer **P2** was synthesized using monomers **M2** (0.239 g, 0.2 mmol) and **D1** (0.248 g, 0.2 mmol). Yield – 86%. M<sub>w</sub>= 134 kDa, M<sub>w</sub>/M<sub>n</sub>=1.5

#### **Polymer P3**

Polymer **P3** was synthesized using monomers **M3** (0.256 g, 0.2 mmol) and **D1** (0.248 g, 0.2 mmol). Yield – 82%. M<sub>w</sub>= 168 kDa, M<sub>w</sub>/M<sub>n</sub>=1.5

#### **Polymer P4**

Polymer **P4** was synthesized using monomers **M4** (0.272 g, 0.2 mmol) and **D1** (0.248 g, 0.2 mmol). Yield – 87%. M<sub>w</sub>= 235 kDa, M<sub>w</sub>/M<sub>n</sub>=2.2

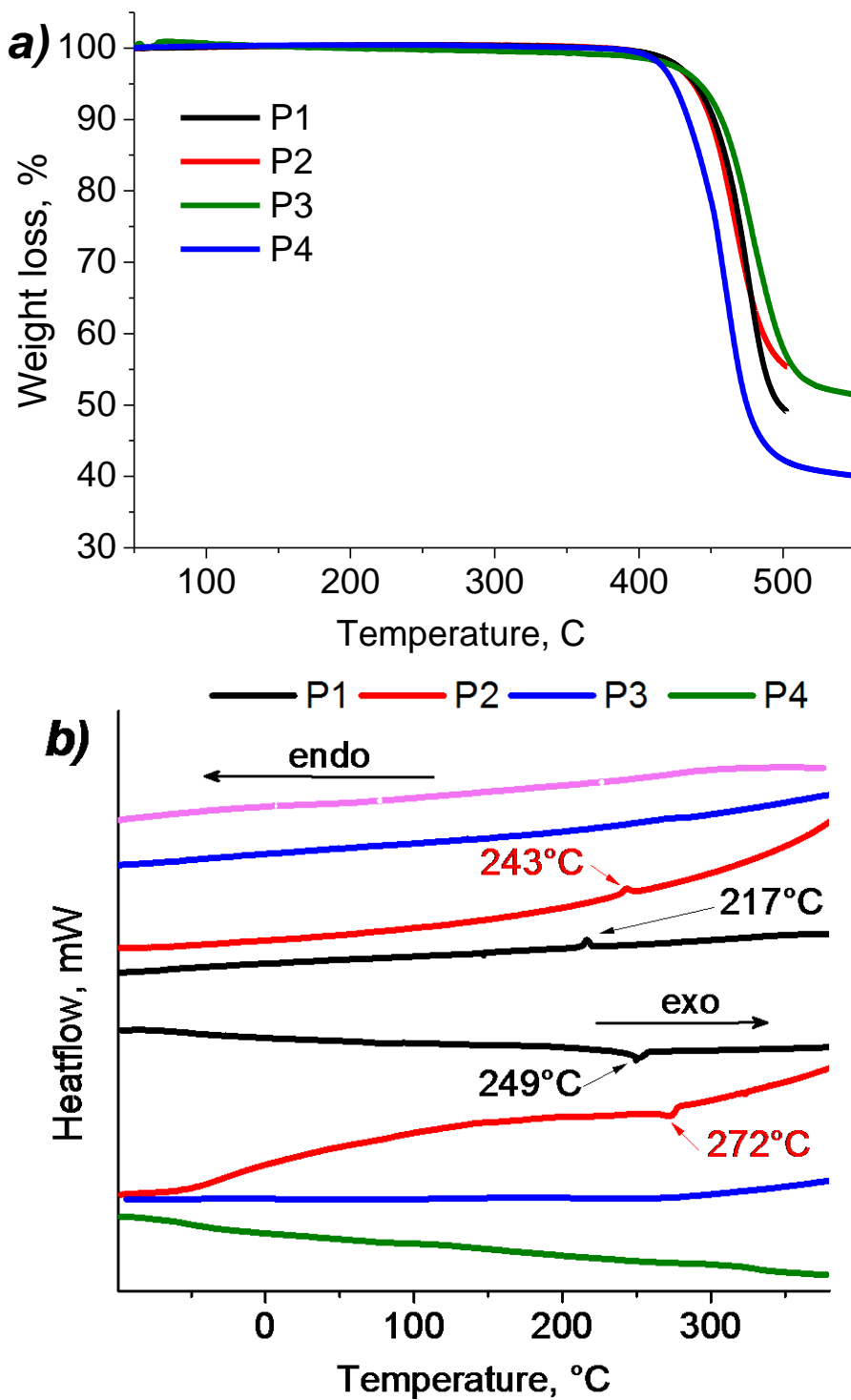


Fig. S1. TGA (**a**) and DSC (**b**) curves for conjugated polymers **P1-P4** (heating rate 15 °C/min under N<sub>2</sub> atmosphere)

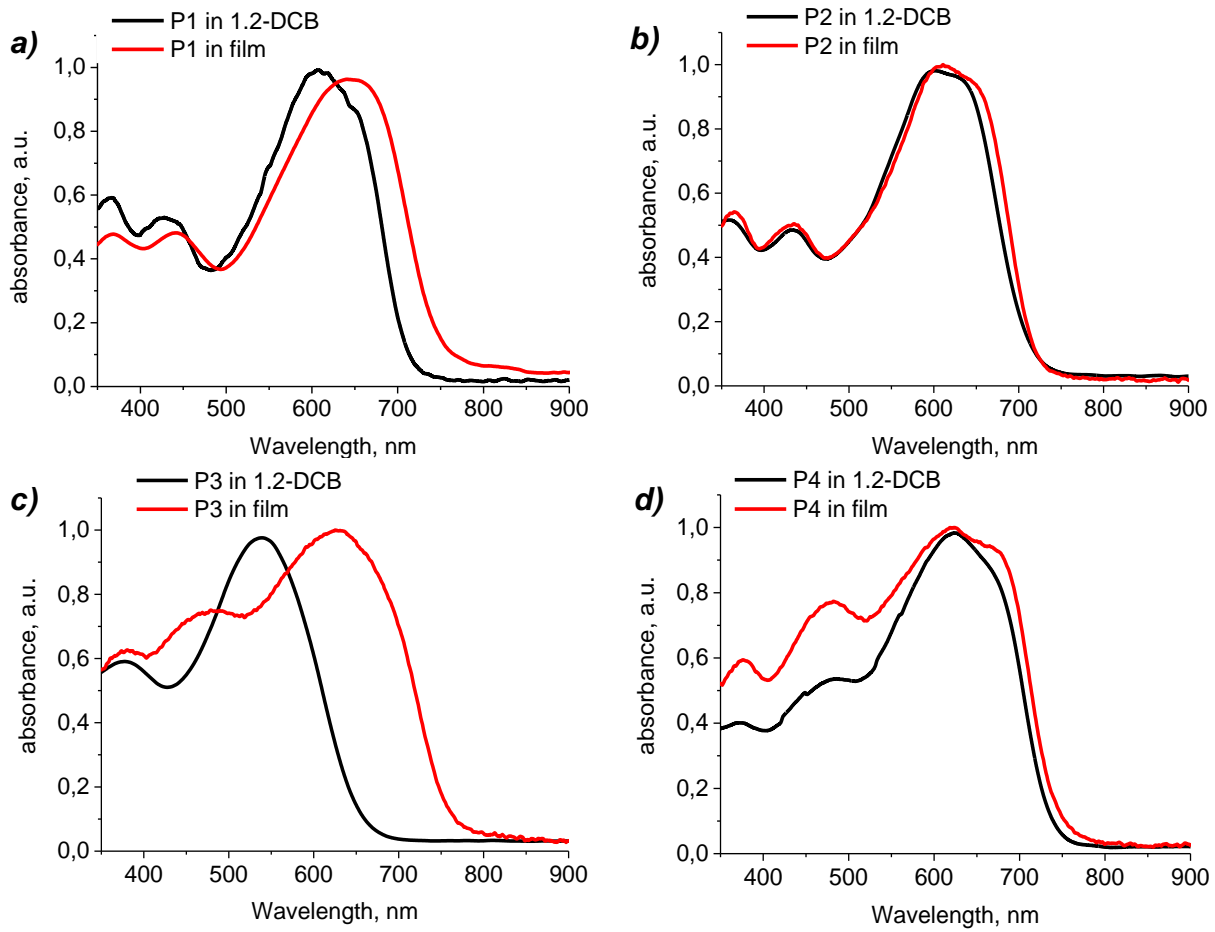


Fig. S2. Absorption spectra of polymers **P1-P4** in solution and in thin films.

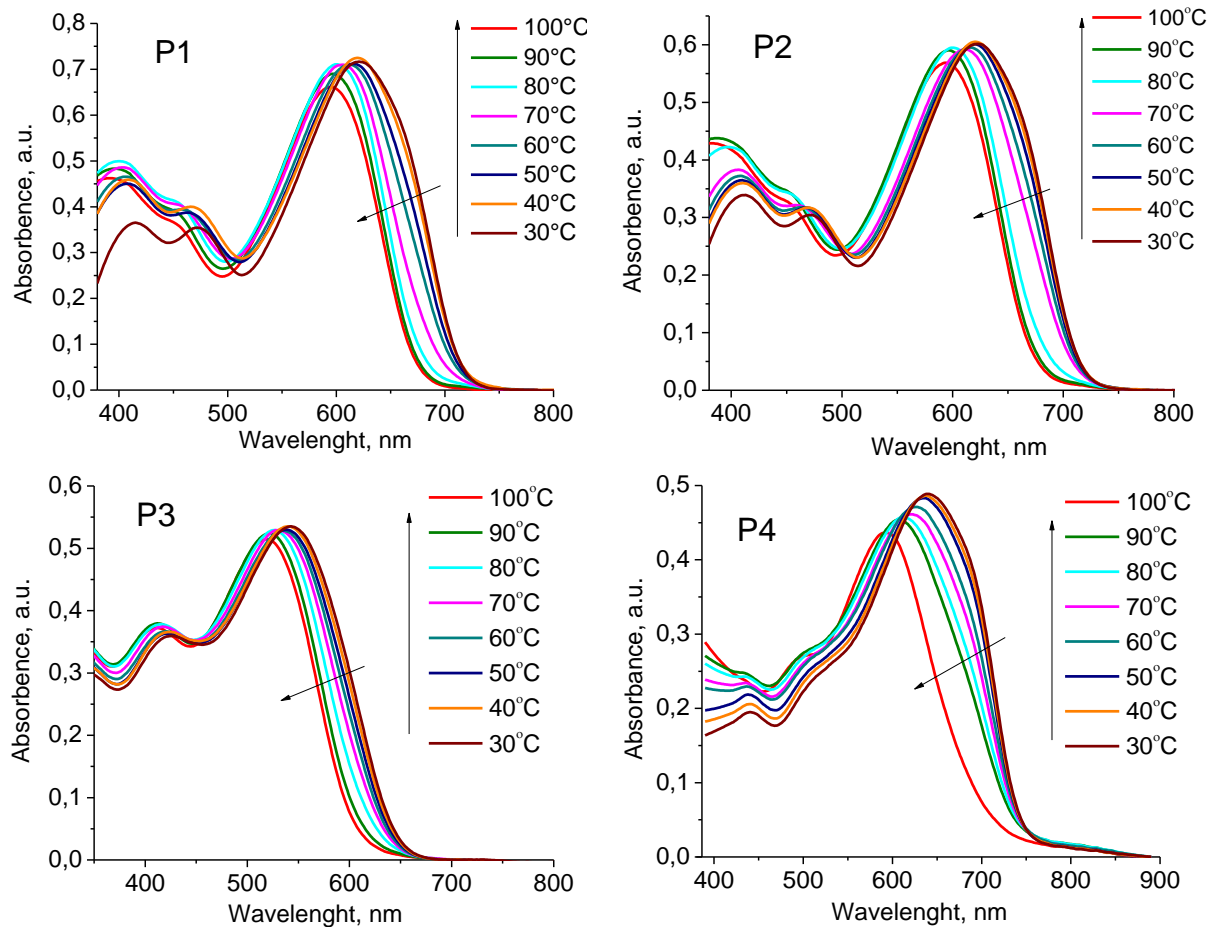


Fig. S3. Temperature-dependent UV-vis absorption spectra of the polymers **P1-P4** in 1,2-DCB solution.

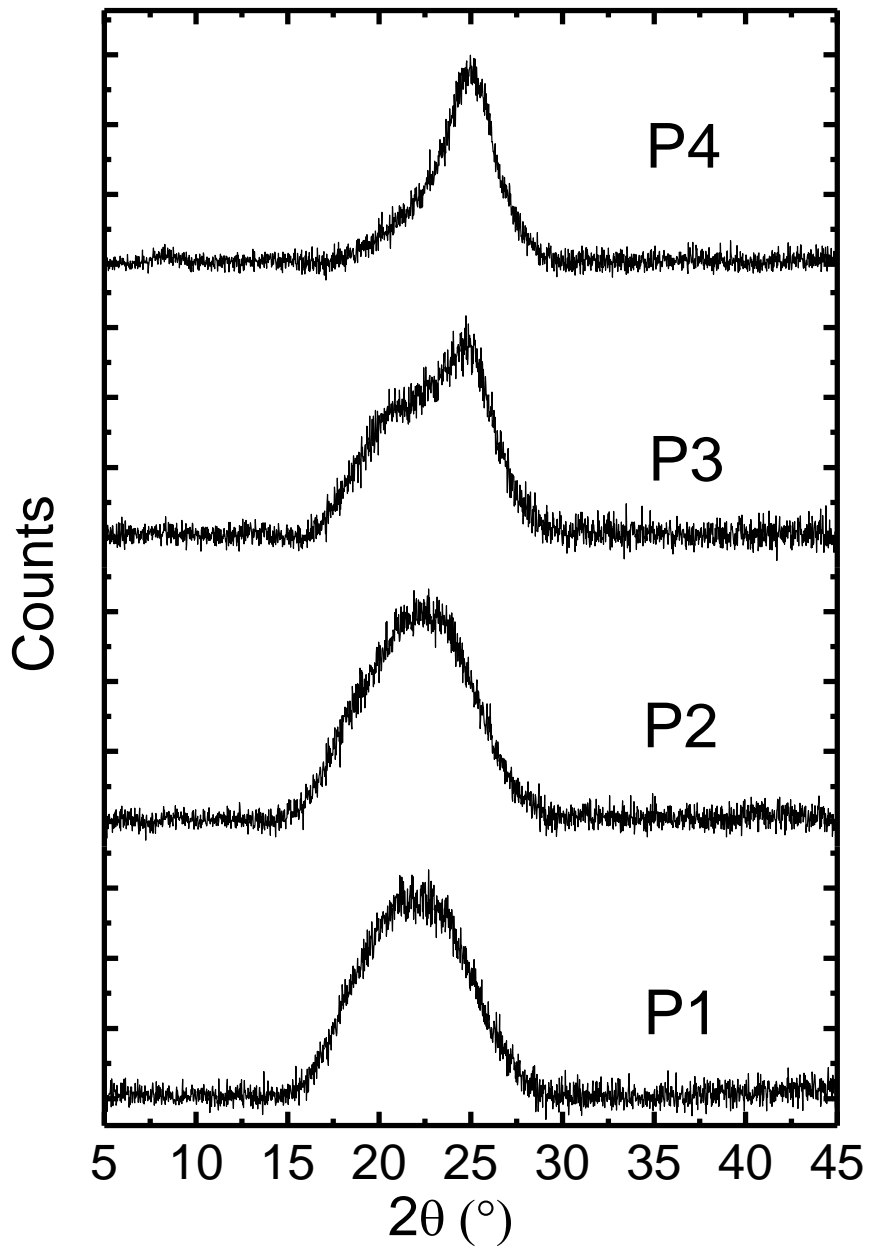


Fig. S4. XRD profiles of the pristine polymers **P1-P4**

### Optimization of devices based on P1/[70]PCBM blends

Table S1. Parameters of devices based on **P1**/[70]PCBM blends processed with different D:A ratio.

D:A ratio	V <sub>OC</sub> , mV	J <sub>SC</sub> , mA/cm <sup>2</sup>	FF, %	η <sub>max</sub> , %	η <sub>aver</sub> <sup>a)</sup> , %
1:0.5	761	3.4	36	1.0	0.9
1:1	824	5.8	58	2.8	2.7
1:2	787	5.4	32	1.3	1.2

<sup>a)</sup> Average PCE obtained from eight devices

Table S2. Parameters of devices based on **P1**/[70]PCBM blends processed with fixed D:A ratio of 1:1 and different active layer thicknesses.

Blends film thickness, nm	V <sub>OC</sub> , mV	J <sub>SC</sub> , mA/cm <sup>2</sup>	FF, %	η <sub>max</sub> , %	η <sub>aver</sub> <sup>a)</sup> , %
130	813	6.8	57	3.2	3.1
180	816	7.4	56	3.4	3.2
220	832	5.8	57	2.8	2.6

<sup>a)</sup> Average PCE obtained from eight devices

Table S3. Parameters of devices based on **P1**/[70]PCBM blends processed with fixed D:A ratio of 1:1, blends film thickness of 180 nm and different annealing temperature (annealing time 10 min).

Temperature, °C	V <sub>OC</sub> , mV	J <sub>SC</sub> , mA/cm <sup>2</sup>	FF, %	η <sub>max</sub> , %	η <sub>aver</sub> <sup>a)</sup> , %
60	827	7.2	52	3.1	3.0
95	812	7.4	56	3.3	3.2
120	745	5.3	47	1.8	1.6

<sup>a)</sup> Average PCE obtained from eight devices

Table S4. Parameters of devices based on **P1**/[70]PCBM blends processed with fixed D:A ratio of 1:1 blends film thickness of 180 nm, annealing temperature (annealing time 10 min) 95°C and SVA post treatment.

SVA	V <sub>OC</sub> , mV	J <sub>SC</sub> , mA/cm <sup>2</sup>	FF, %	η <sub>max</sub> , %	η <sub>aver</sub> <sup>a)</sup> , %
w/o	817	7.6	50	3.1	3.0
CHCl <sub>3</sub>	810	8.5	49	3.4	3.1

<sup>a)</sup> Average PCE obtained from eight devices

### Optimization of devices based on P2/[70]PCBM blends

Table S5. Parameters of devices based on **P2/[70]PCBM** blends processed with different D:A ratio.

D:A ratio	V <sub>OC</sub> , mV	J <sub>SC</sub> , mA/cm <sup>2</sup>	FF, %	η <sub>max</sub> , %	η <sub>aver</sub> <sup>a)</sup> , %
1:0.5	849	2.6	59	1.3	1.1
1:1	860	3.2	52	1.4	1.3
1:2	828	1.8	51	0.8	0.7

<sup>a)</sup> Average PCE obtained from eight devices

Table S6. Parameters of devices based on **P2/[70]PCBM** blends processed with fixed D:A ratio of 1:1 and different active layer thicknesses.

Blends film thickness, nm	V <sub>OC</sub> , mV	J <sub>SC</sub> , mA/cm <sup>2</sup>	FF, %	η <sub>max</sub> , %	η <sub>aver</sub> <sup>a)</sup> , %
140	803	2.3	41	0.8	0.7
185	841	3.4	52	1.5	1.4
220	817	2.7	42	1.0	0.8

<sup>a)</sup> Average PCE obtained from eight devices

Table S7. Parameters of devices based on **P2/[70]PCBM** blends processed with fixed D:A ratio of 1:1, blends film thickness of 185 nm and different annealing temperature (annealing time 10 min).

Temperature, °C	V <sub>OC</sub> , mV	J <sub>SC</sub> , mA/cm <sup>2</sup>	FF, %	η <sub>max</sub> , %	η <sub>aver</sub> <sup>a)</sup> , %
w/o	801	2.9	37	0.9	0.8
60	826	3.0	48	1.2	0.8
95	872	3.3	52	1.5	1.4
120	796	2.4	47	0.9	0.9

<sup>a)</sup> Average PCE obtained from eight devices

### Optimization of devices based on P3/[70]PCBM blends

Table S8. Parameters of devices based on **P3/[70]PCBM** blends processed with different D:A ratio.

D:A ratio	V <sub>OC</sub> , mV	J <sub>SC</sub> , mA/cm <sup>2</sup>	FF, %	η <sub>max</sub> , %	η <sub>aver</sub> <sup>a)</sup> , %
1:1	731	8.7	45	2.8	2.7
1:2	736	8.6	52	3.3	3.2
1:3	696	4.1	38	1.1	1.0

<sup>a)</sup> Average PCE obtained from eight devices

Table S9. Parameters of devices based on **P3/[70]PCBM** blends processed with fixed D:A ratio of 1:2 and different active layer thicknesses.

Blends film thickness, nm	V <sub>OC</sub> , mV	J <sub>SC</sub> , mA/cm <sup>2</sup>	FF, %	η <sub>max</sub> , %	η <sub>aver</sub> <sup>a)</sup> , %
120	730	7.8	54	3.0	2.8
155	726	8.6	55	3.5	3.4
180	649	8.6	53	3.0	3.0

<sup>a)</sup> Average PCE obtained from eight devices

Table S10. Parameters of devices based on **P3/[70]PCBM** blends processed with fixed D:A ratio of 1:2, blends film thickness of 155 nm and different annealing temperature (annealing time 10 min).

Temperature, °C	V <sub>OC</sub> , mV	J <sub>SC</sub> , mA/cm <sup>2</sup>	FF, %	η <sub>max</sub> , %	η <sub>aver</sub> <sup>a)</sup> , %
60	683	9.0	48	2.9	2.6
95	723	9.1	53	3.5	3.4
120	714	9.3	39	2.6	2.3

<sup>a)</sup> Average PCE obtained from eight devices

## Optimization of devices based on **P4/[70]PCBM** blends

Table S11. Parameters of devices based on **P4**/[70]PCBM blends processed with different D:A ratio.

D:A ratio	V <sub>OC</sub> , mV	J <sub>SC</sub> , mA/cm <sup>2</sup>	FF, %	η <sub>max</sub> , %	η <sub>aver</sub> <sup>a)</sup> , %
1:0.5	750	10.9	45	3.6	3.5
1:1	762	11.2	43	3.7	3.6
1:2	731	8.7	45	2.8	2.7

<sup>a)</sup> Average PCE obtained from eight devices

Table S12. Parameters of devices based on **P4**/[70]PCBM blends processed with fixed D:A ratio of 1:1 and different active layer thicknesses.

Blends film thickness, nm	V <sub>OC</sub> , mV	J <sub>SC</sub> , mA/cm <sup>2</sup>	FF, %	η <sub>max</sub> , %	η <sub>aver</sub> <sup>a)</sup> , %
115	755	7.8	60	3.6	3.4
150	766	8.9	56	3.8	3.7
180	726	8.6	55	3.5	3.4

<sup>a)</sup> Average PCE obtained from eight devices

Table S13. Parameters of devices based on **P4**/[70]PCBM blends processed with fixed D:A ratio of 1:1, blends film thickness of 150 nm, and different annealing temperature (annealing time 10 min).

Temperature, °C	V <sub>OC</sub> , mV	J <sub>SC</sub> , mA/cm <sup>2</sup>	FF, %	η <sub>max</sub> , %	η <sub>aver</sub> <sup>a)</sup> , %
60	751	12.3	53	4.9	4.8
95	759	11.9	55	5.0	4.9
110	742	11.4	58	4.9	4.8

<sup>a)</sup> Average PCE obtained from eight devices

Table S14. Parameters of devices based on **P4**/[70]PCBM blends processed with fixed D:A ratio of 1:1, blends film thickness of 150 nm, annealing temperature of 95°C, and different additives 0.5% vol.

Additives	V <sub>OC</sub> , mV	J <sub>SC</sub> , mA/cm <sup>2</sup>	FF, %	η <sub>max</sub> , %	η <sub>aver</sub> <sup>a)</sup> , %
w/o	738	10.8	50	4.0	3.8
CN	731	9.9	51	3.7	3.6
ODT	766	12.1	55	5.1	5.0
DIO	723	12.3	54	4.8	4.7

<sup>a)</sup> Average PCE obtained from eight devices

CN – 1-chloronaphthalene; ODT – 1,8-octanedithiol; DIO – 1,8-diiodooctane.

Table S15. Parameters of devices based on **P4**/[70]PCBM blends processed with the fixed D:A ratio of 1:1, blends film thickness of 150 nm, annealing temperature of 95°C, and using additive ODT with various concentrations.

Additives	V <sub>OC</sub> , mV	J <sub>SC</sub> , mA/cm <sup>2</sup>	FF, %	η <sub>max</sub> , %	η <sub>aver</sub> <sup>a)</sup> , %
w/o	740	10.6	51	4.0	3.9

ODT 0.5 vol%	731	13.2	52	5.0	4.9
ODT 1 vol%	720	15.7	62	7.0	6.5
ODT 3 vol%	738	11.5	52	4.4	4.2

a) Average PCE obtained from eight devices

## S2. Structural definitions

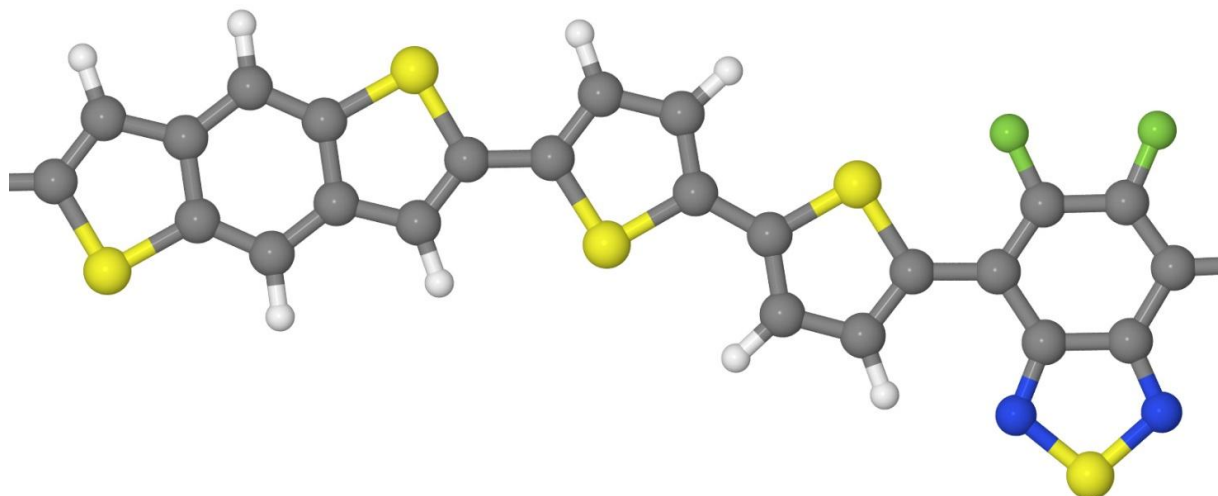
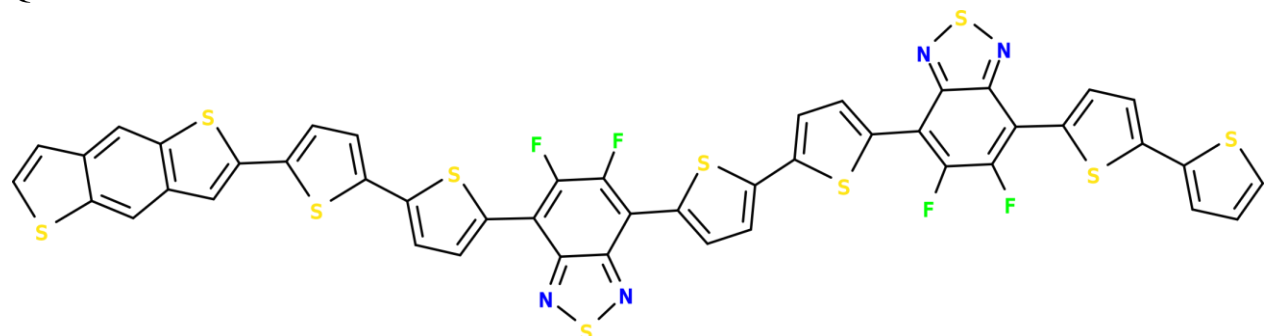


Fig. S5 Fragment of a polymer showing all considered building blocks in their energetically most favorable interconnection (in some polymers fluorine atoms are replaced by hydrogens). Note that inter-thiophene dihedrals are nonplanar in the energy minimum. Block notations: 'D' for benzodithiophene, 'T' for thiophene, 'F' for fluorinated benzothiadiazole, 'B' for benzothiadiazole. In these notations the shown fragment can be written as 'DTTF' or 'DT2F'.

Q1



Q2

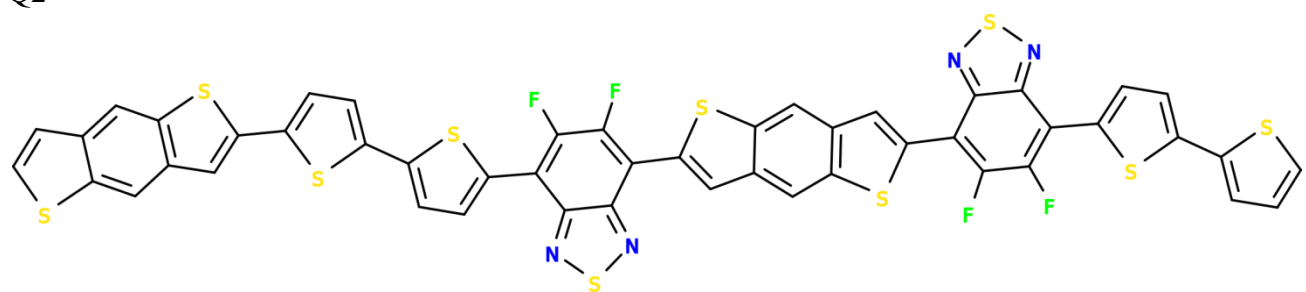


Fig. S6a. Reference polymers Q1=T2FT2FT2 (top) and Q2=T2FDFT2 (bottom). These polymers are minimal structural variations of **P4** with linear structure.

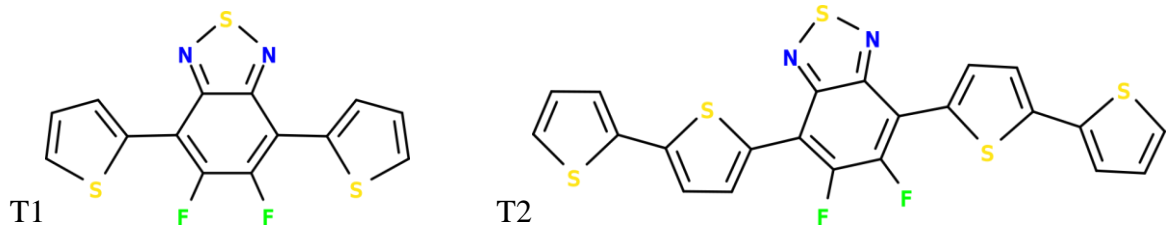


Fig. S6b. Reference polymers T1=TFT=PffBT2T (left) and T2=T2FT2=PffBT4T (right). The polymer T2 is currently the best performing polymer [6,7] based on the considered set of building blocks. The T1 is the variation of T1 with the smallest repeating unit.

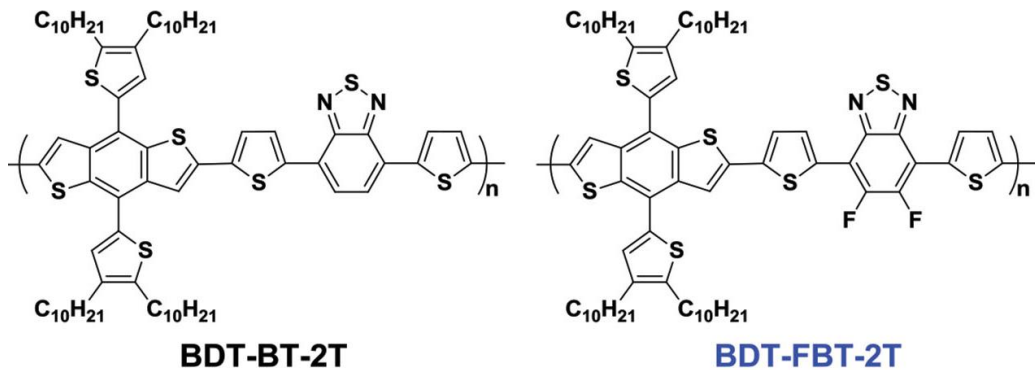


Fig. S6c. Reference polymers U1=DTBT (left) and U2=DTFT (right) [8]. These polymers are minimal structural variations of **P1-P4** with the smallest repeating unit.

### S3. PCE parameters

Table S16. PCE parameters: measurements and analysis [9] (blue stands for experiment, black - for theory). For polymers **P1-P4** the LUMO energy is estimated from HOMO energy (by CV) and optical gap.

parameter	units	P1	P2	P3	P4	U1	U2	T2
$\lambda_{\max}(\text{solution})$	nm	606	602	538	623	609	631	-
$E_g(\text{optical})$	eV	1.67	1.73	1.63	1.66	1.68	1.72	1.65
PCE <sub>max</sub> ( $E_g$ )	%	38.9	37.4	40.2	39.2	38.6	37.6	39.5
PCE	%	3.4	1.5	3.5	7.0	5.4	7.7	11.3
$V_{\text{OC}}$	V	0.843	0.872	0.723	0.720	0.750	0.850	0.784
$V_{\text{OC}}/E_g$	%	50.5	50.4	44.4	43.4	44.6	49.4	47.5
$J_{\text{SC}}$	$\text{mA/cm}^2$	8.5	3.3	9.1	15.7	11.2	13.3	19.8
$J_{\text{SC}}/J_{\text{SC}}^{\text{max}}$	%	36.5	15.3	36.9	66.4	48.7	60.8	82.7
FF	%	48	52	53	62	64	68	73
4.15+LUMO	eV	0.25	0.17	0.31	0.3	0.61	0.53	-

#### S4. Computational methodology

All computations are carried out in Gaussian 16 program suite [10]. Density Functional Theory (DFT) and time-dependent DFT (TDDFT) frameworks are used for calculations of ground and excited state electronic properties, respectively. Used for the majority of calculations in present work, CAM-B3LYP is a long-range corrected hybrid functional known to provide a correct description of molecular and electronic structure of extended  $\pi$ -conjugated systems [11–13]. Majority of computations for free molecules is made in 6-31G\* basis set. The solvent effects are taken into account using the conductor-like polarizable continuum model [14–17] (CPCM) with the dielectric constant  $\epsilon_{\text{static}}=4.7$  (chloroform) close to upper limit of typical dielectric environment of bulk conjugated polymers [6]. Electronic absorption spectra were modeled using TD-DFT results and gaussian broadening (Fig. S10).

In order to model electronic properties of polymers studied in present work, we use donor- and acceptor-centered oligomers as shown in Fig. S9. Aliphatic chains have been removed since they have minor impact on electronic excitation / charge transfer energies for the lowest state relevant for experimental investigation (frontier molecular orbitals are localized on conjugation backbone only). All geometry optimizations were performed supposing planar conduction backbone as a model of a statistically averaged conformation. Values for dihedrals were chosen to a) correspond to the lowest-energy planar configuration for the dimer (Table S18) and b) not introduce considerable steric effects. Thiophenes attached by single C-C bond to benzodithiophene fragment have also been omitted since taking them into account does not introduce significant changes in electronic properties of polymer (look at Table S21 - and compare with differences for dithiophenylbenzodithiophene molecule) but reduce conformational rigidity; moreover, those rings won't allow for planar structure thus reducing the symmetry of those oligomers. Main descriptors for electronic structure used in present work are frontier orbitals energies, ionization potential and electron affinity, energy gap ( $S_0-S_1$  vertical transition energy). Since changes in HOMO closely follow those in IP as shown in Table S19 (as should be expected), for the latter study charge-related phenomena could be described using just frontier orbitals. Taking into account solvent effects does not induce considerable changes in trends for energy gap and ionization potential. Thus, in zero approximation these could be omitted.

## S5. Properties of building blocks and their interconnections

Table S17. Variation of the energy (in eV, sign is ignored) of LMOs (localized molecular orbitals) of the building blocks in different interconnections sampled over a set of several polymers (DF, DFT2F, DFTF, DTFT, DTFTFT, DTFT2FT, DT2FTFT2, DT2FT2FT2D, DT2FDFT2). Root mean square deviations in geometry do not exceed 0.005 Å. The column "free" lists MO energies for the corresponding free molecule in vacuum; "nodes" column shows nodal pattern of the wave-function (number of lobes in along-polymer and across-polymer directions). The first non- $\pi$  MO of the free molecule is also listed.

#	free	min	average	max	sym	nodes	localization
benzoDithiophene							
1	6.77	6.92	6.97(3)	7.03	Bg	3x2	
2	7.56	7.76	7.80(3)	7.87	Bg	4x1	
3	8.38	8.53	8.58(3)	8.64	Au	2x2	
4	9.76	9.87	9.91(3)	9.96	Bg	1x2	
5	9.98	10.13	10.16(3)	10.21	Au	3x1	
	10.63						non- $\pi$
6	12.02	12.15	12.18(3)	12.23	Bg	2x1	
7	13.17	13.28	13.32(3)	13.36	Au	1x1	
Thiophene							
1	7.87	8.49	8.57(3)	8.63	A2	2x1	double bonds
2	8.22	8.47	8.59(4)	8.68	B1	1x2	S and single bond
	10.90						non- $\pi$
3	12.10	12.39	12.46(3)	12.53	B1	1x1	delocalized
Fluorinated benzothiadiazole							
1	8.37	8.72	8.77(4)	8.85	A2	2x3	
2	8.62	8.82	8.86(2)	8.91	B1	1x4	
	10.17						non- $\pi$
3	11.08	11.31	11.35(3)	11.41	A2	2x2	
4	11.37	11.54	11.58(3)	11.64	B1	1x3	
5	14.50	14.70	14.74(3)	14.80	B1	1x2	
6	14.66	14.77	14.81(2)	14.86	A2	2x1	
7	15.75	15.90	15.94(3)	16.00	B1	1x1	

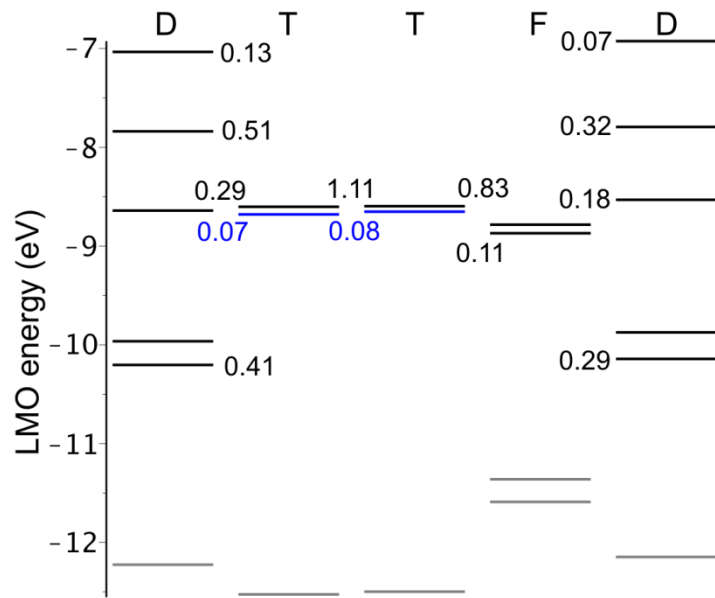


Fig. S7a. LMO interaction diagram for all possible interconnections between the building blocks sampled in the polymer with the repeating unit 'DT2FDFT2'. Numbers indicate renormalized electronic couplings (in eV) for holes: those in black color show couplings to the highest LMO of the adjacent block, numbers in blue colors show couplings to or between the blue-colored LMOs. Electronic coupling  $t$  between a pair of orbitals with energy difference  $\varepsilon$  are renormalized according to the formula  $t'=t\cdot\sqrt{[1-1/\sqrt{1+4t^2/\varepsilon^2}]}$ , which gives exact level shifts  $t'$  for the two-level system. All couplings larger than 0.05 eV are listed. Levels in gray color are too deep for transport and also intermix with non- $\pi$  orbitals intervening below -10 eV.

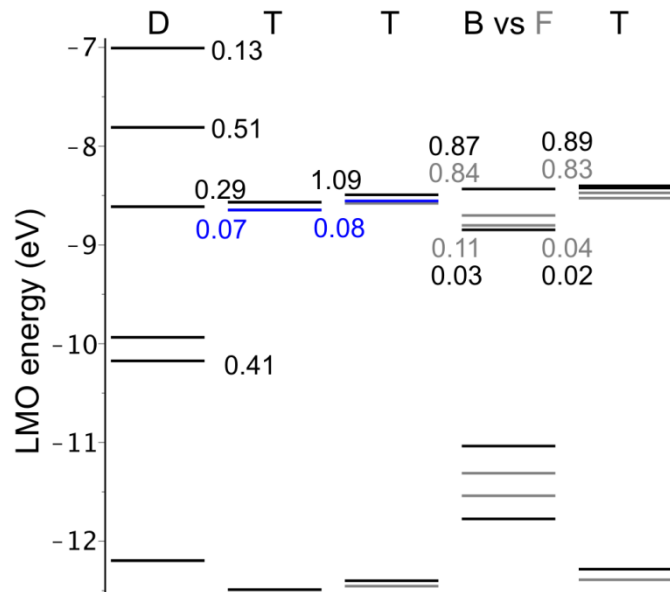


Fig. S7b. LMO interaction diagram of **P3** (black and blue colors) vs. **P4** (gray color) polymers.

Table S18. Conformational properties (calculated by CAM-B3LYP/6-31G\*) of all reasonable interconnections of the considered building blocks. The two possible rotamers are denoted as 1 and 2, where 1 corresponds to the lowest energy rotamer. Abbreviation "in clf" means PCM calculations with dielectric constant of chloroform.  $\Delta E = E_2 - E_1$  where  $E_{1,2}$  is the energies of the two rotamers at fully relaxed geometry.  $\Delta HOMO/LUMO$  are defined in the same way.

<b>parameter</b>	<b>units</b>	<b>D+D</b>	<b>D+T</b>	<b>T+T</b>	<b>T+B</b>	<b>T+F</b>	<b>D+F</b>
dihedral 1 (stable)	deg.	9	19	26	10	0	0
dihedral 2 (metastable)	deg.	31	31	35	21	0	0
dihedral 1 dispersion at 300K	deg.	25	28	38	23	18	19
dihedral 2 dispersion at 300K	deg.	35	36	32	28	21	23
planarization energy 1		0.1	2.5	7.8	0.3	0	0
planarization energy 2	meV	23.3	21.0	24.9	6.7	0	0
rotational barrier	meV	148	124	99	170	187	179
barrier in clf	meV	148	126	103	141	154	147
$\Delta E = E_2 - E_1$	meV	48	36	28	33	28	36
$\Delta E$ in clf	meV	43	32	25	13	21	26
rotamers ratio at 300K		5.8	3.9	3.0	3.3	2.2	3.0
frequency 1	meV	1.1	3.2	4.7	2.0	3.7	2.2
frequency 2	meV	3.1	4.4	5.6	3.9	1.0	0.7
frequency 1 planar	meV	-0.8	-2.5	-3.9	-1.6	3.7	2.2
frequency 2 planar	meV	-3.5	-4.5	-5.4	-3.6	1.0	0.7
frequency at barrier	meV	-4.0	-5.3	-6.0	-5.4	-4.6	-2.9
$\Delta HOMO$	eV	+0.02	+0.03	+0.07	+0.00	-0.02	-0.03
$\Delta LUMO$	eV	-0.11	-0.08	-0.08	-0.03	-0.00	-0.01

## S6. Electronic properties

Fig. S8. Types of oligomers considered in electronic properties calculations for **P1-P4** and **U1-2** systems.

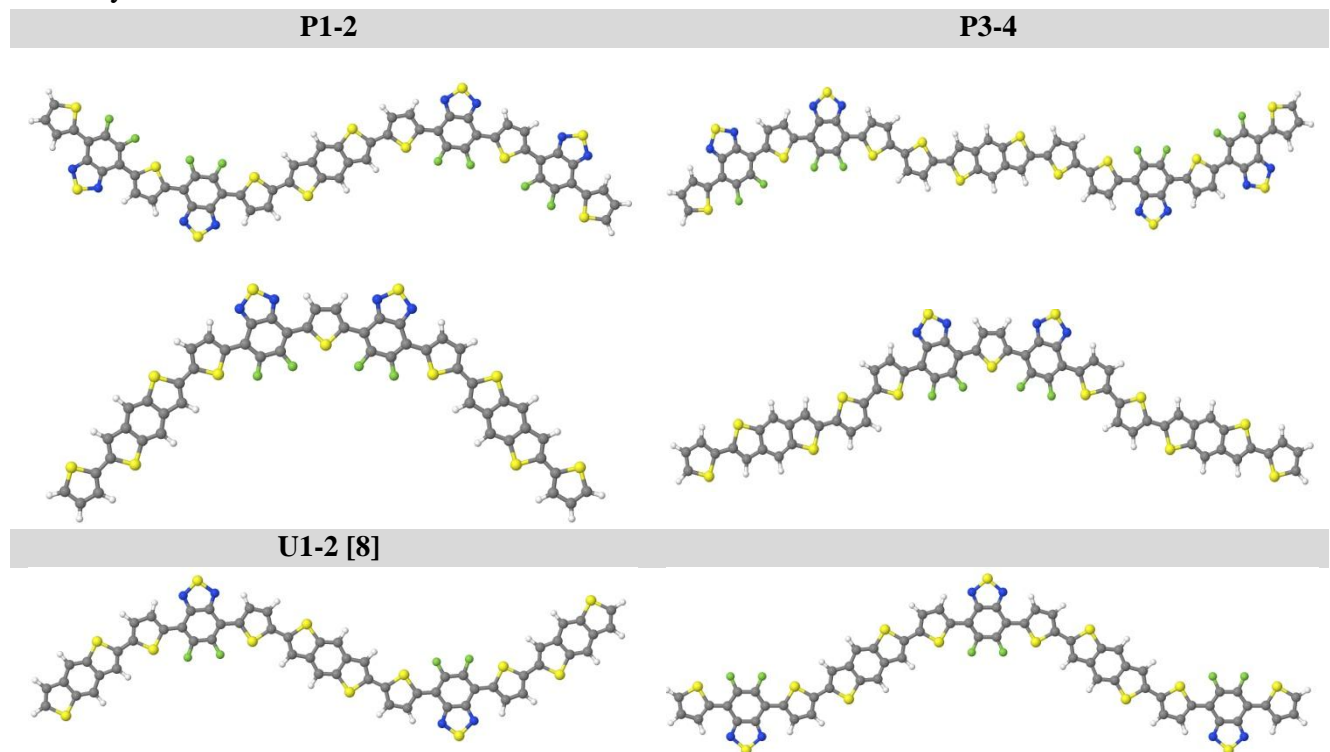


Fig. S9a. Natural transition orbitals (for S<sub>0</sub>-S<sub>1</sub> transition) for donor-centered oligomer of **P4** polymer in vacuum and in chloroform.

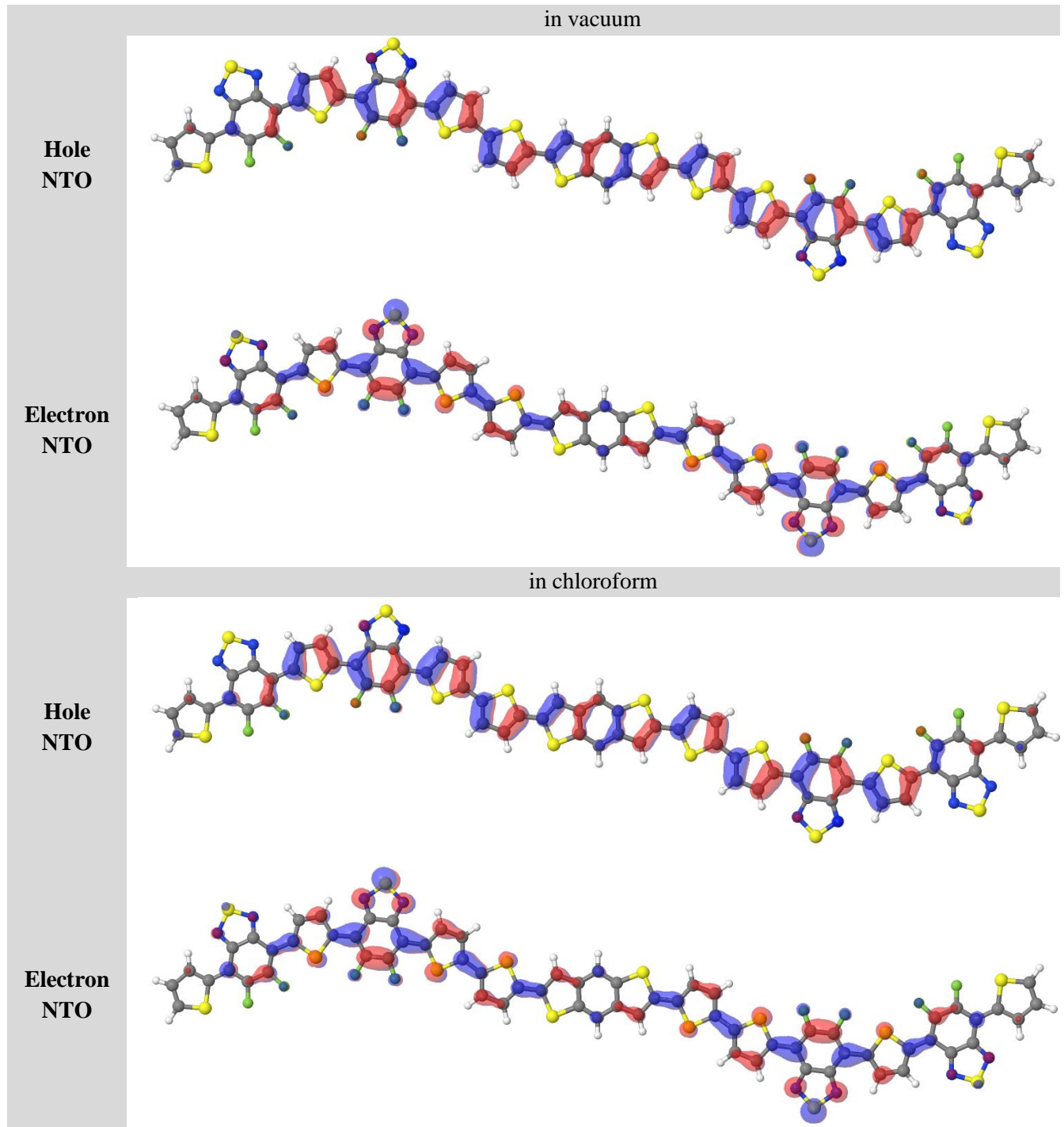


Fig. S9b. Natural transition orbitals (for  $S_0$ - $S_1$  transition) for acceptor-centered oligomer of **P4** polymer in vacuum and in chloroform.

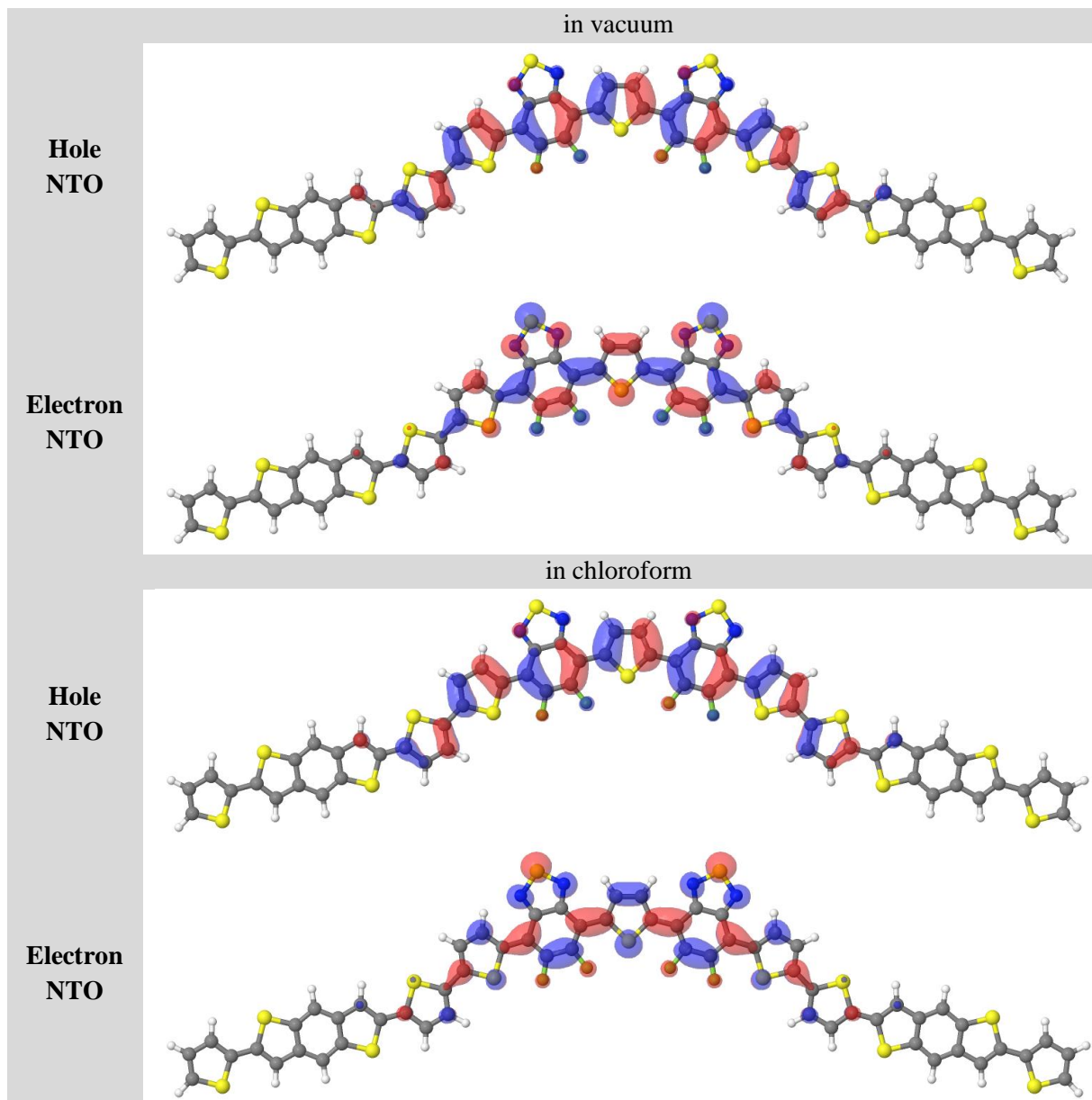


Fig. S9c. Natural orbitals for **P4** oligomers computed at cation (for donor-oriented oligomer) and anion (for acceptor-oriented oligomer) geometries in gas and in chloroform.

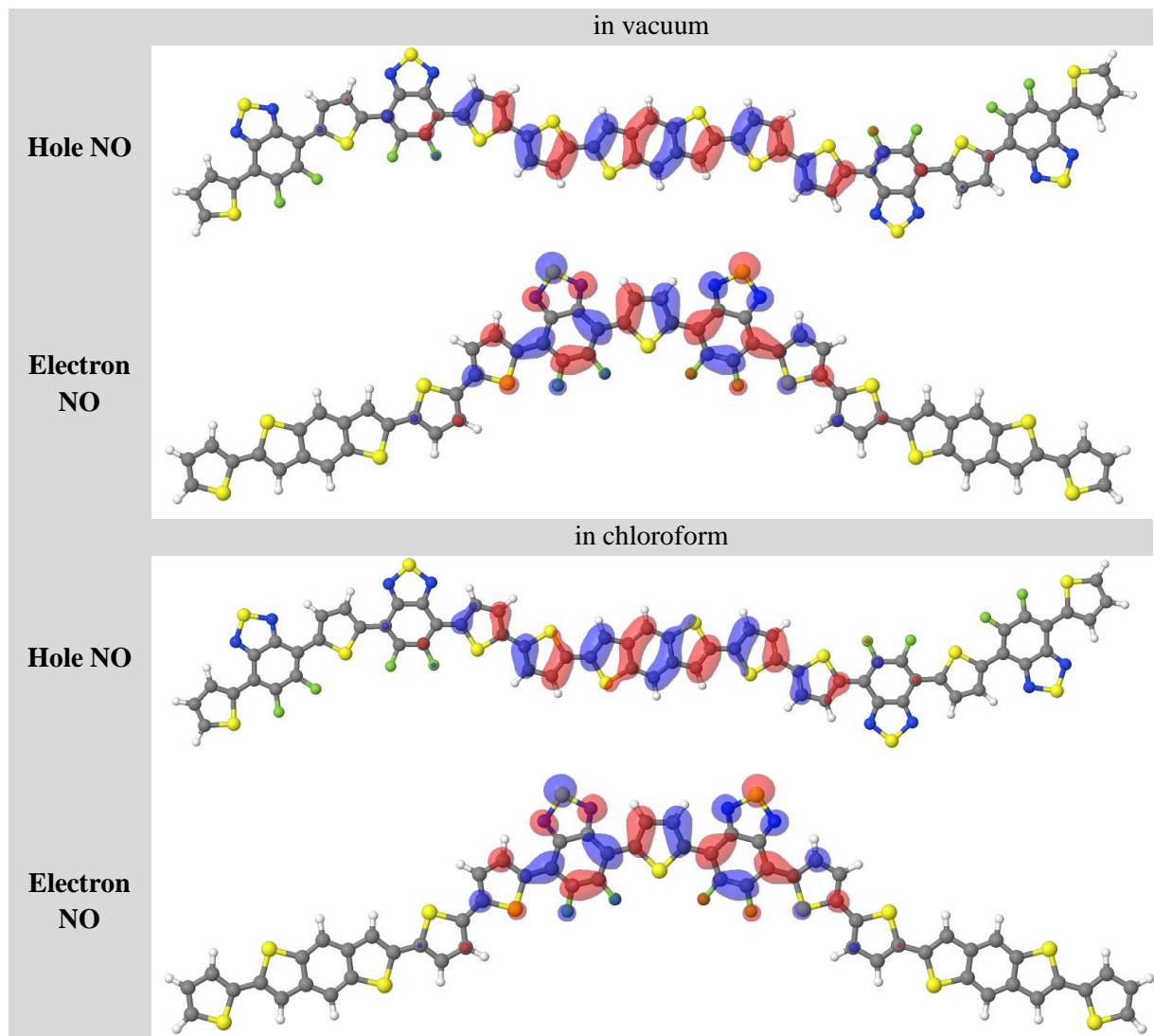


Fig. S10. Electronic absorption spectra for different fragments of **P1-P4** conjugated polymers computed by TD-DFT CAM-B3LYP/6-31G\* in vacuum. Differently coloured lines correspond to differently centered oligomers (see Fig. S9).

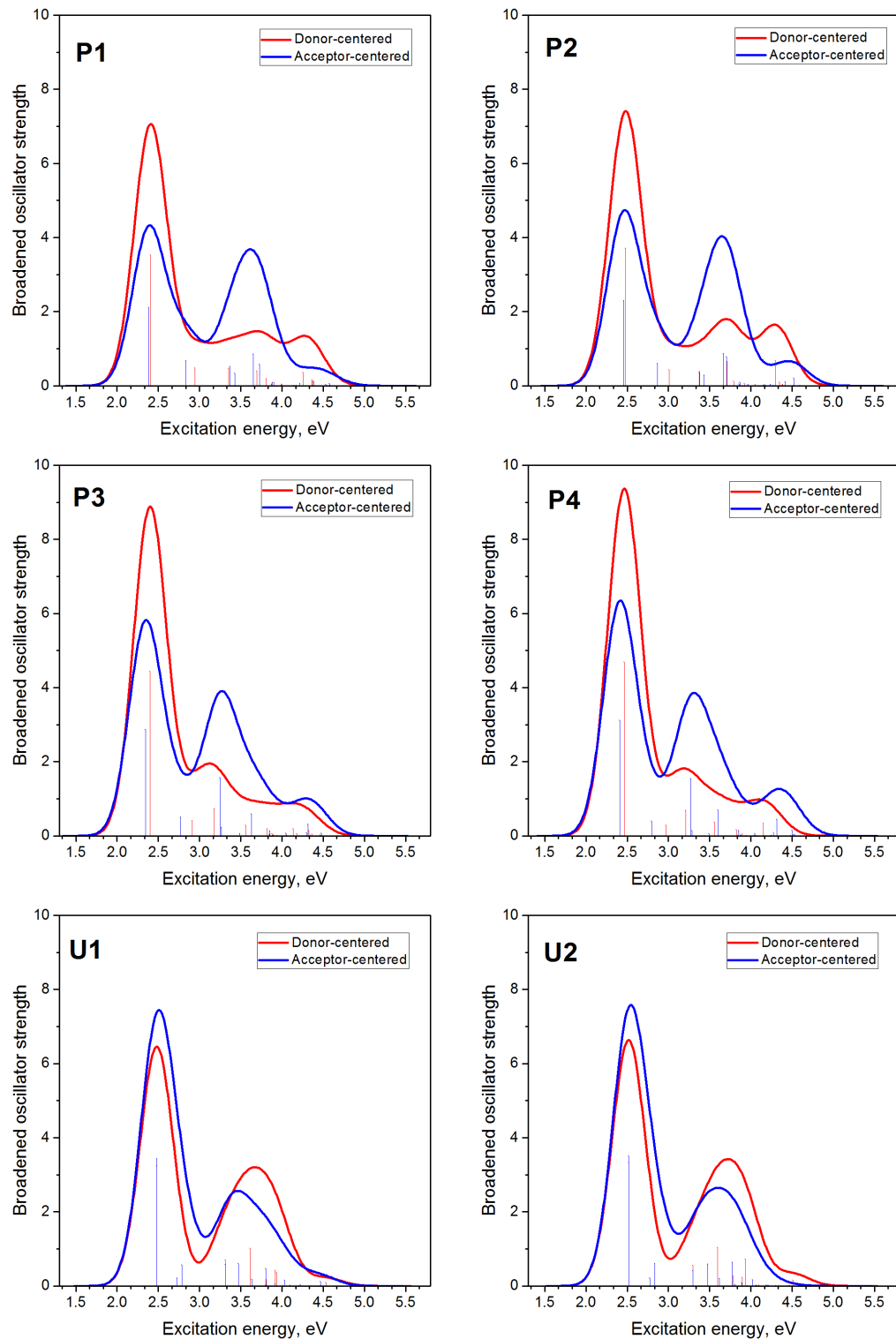


Table S19. Experimental and calculated (CAM-B3LYP /6-31G\* for different oligomers) trends for energy gap and frontier orbital energies (in eV). Here "clf" means that solvent (namely, chloroform) effects were taken into account using CPCM solvation model, whereas "vac" means that calculations were made for isolated molecule.

parameter	P1	P2	P3	P4	U1	U2
$\Delta E_g$	0.01	0.07	-0.03	0	0.02	0.06
$\Delta E(S_0-S_1)$ in vac	-0.04(1)	0.03(1)	-0.06(3)	0.00(3)	0.05(0)	0.08(0)
$\Delta E(S_0-S_1)$ in clf	-0.05(1)	0.03(1)	-0.08(3)	0.00(3)	0.04(0)	0.09(0)
$\Delta HOMO$ by CV	0.06	0.2	-0.04	0	-0.33	-0.18
- $\Delta HOMO$	-0.01(1)	0.09(0)	-0.08(0)	0.00(1)	-0.01(1)	0.07(1)
$\Delta IP$ in vac	-0.02(1)	0.09(2)	-0.08(0)	0.00(2)	-0.01(1)	0.07(1)
$\Delta IP$ in clf	-0.05(1)	0.06(5)	-0.09(0)	0.00(7)	-0.04(0)	0.03(2)
- $\Delta LUMO$	0.05	0.13	-0.01	0	-0.35	-0.24
- $\Delta LUMO$	-0.08(1)	0.01(1)	-0.09(3)	0.00(2)	-0.16(1)	-0.08(1)
- $\Delta EA$ in vac	-0.09(3)	0.00(2)	-0.09(3)	0.00(2)	-0.18(0)	-0.10(0)
- $\Delta EA$ in clf	-0.03(13)	0.03(13)	-0.06(16)	0.00(15)	-0.05(14)	0.01(14)

Table S20. Experimental and calculated (CAM-B3LYP /6-31G\* for different oligomers) absolute values of energy gap and frontier orbital energies (in eV).

parameter	P1	P2	P3	P4	U1	U2
Egap optical	1.67	1.73	1.63	1.66	1.68	1.72
$E(S_0-S_1)$ in vac	2.39-2.41	2.46-2.48	2.35-2.40	2.41-2.46	2.48	2.52
-HOMO by CV	5.57	5.71	5.47	5.51	5.18	5.33
-HOMO	6.15-6.16	6.25-6.26	6.09-6.10	6.16-6.18	6.15-6.18	6.22-6.25
IP in vacuum	6.32-6.33	6.42-6.46	6.26-6.27	6.33-6.37	6.33-6.36	6.41-6.43
IP in clf	5.60-5.62	5.67-5.77	5.56-5.57	5.59-5.73	5.62	5.67-5.72
-LUMO by Egap	3.90	3.98	3.84	3.85	3.5	3.61
-LUMO	1.92-1.95	2.01-2.04	1.89-1.94	1.99-2.04	1.84-1.86	1.93-1.94
-EA in vacuum	1.72-1.77	1.81-1.85	1.71-1.78	1.81-1.86	1.65-1.66	1.73-1.74
EA in clf	2.35-2.61	2.41-2.67	2.29-2.60	2.35-2.66	2.32-2.60	2.38-2.65

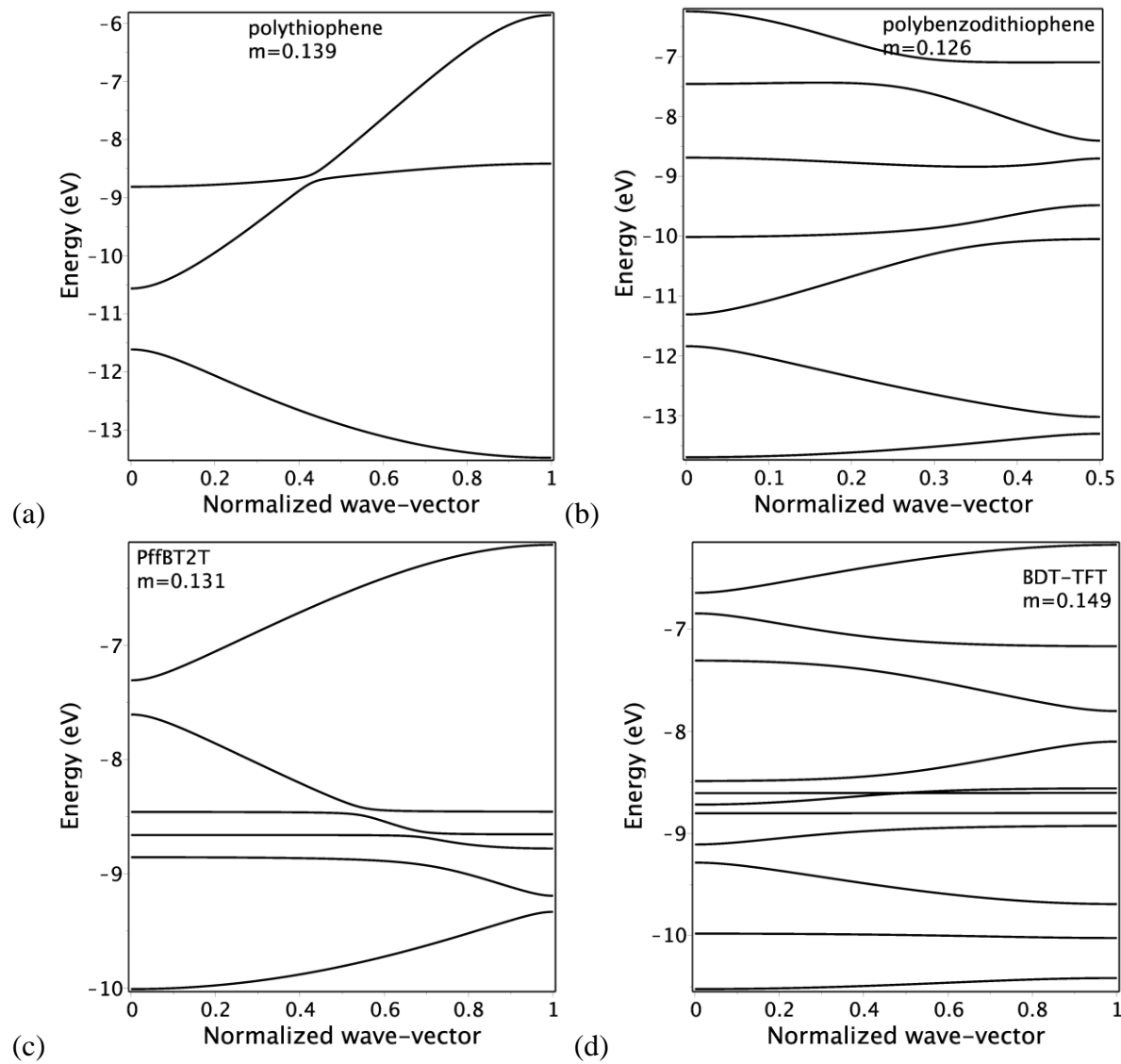


Fig. S11a. Band structure and effective masses for holes in ideal planar reference polymers: (a) 'TT' or polythiophene, (b) 'DD' or polybenzodithiophene, (c) T1=TFT=PffBT2T, (d) U2=DTFT.

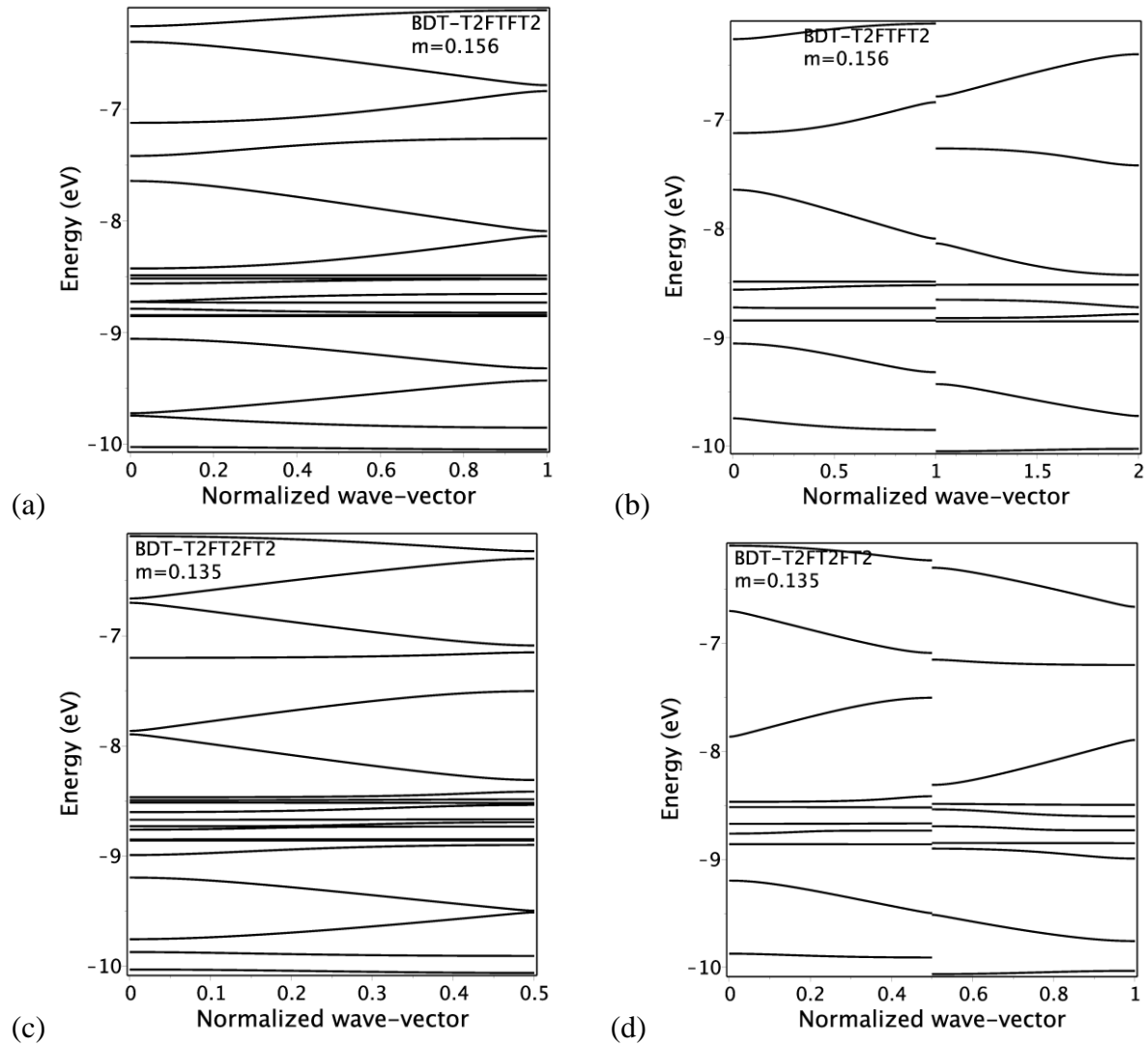


Fig. S11b. Band structure and effective masses for holes in ideal planar polymers: (a,b) P4=DT2FTFT2, (c,d) Q1=DT2FT2FT2. The right panels (b,d) show the band structure unfolded one time. Unit cells of polymers **P1-P4** are so large that the band structure of a single conformer is not meaningful statistically. In particular, the width of the top valence band for **P4** is only 0.15 eV and its separation from the next band is 0.14 eV, so that the band transport is hardly possible even in the ideal polymer. For comparison, 'DT2FT2FT2' has also narrow top valence band (0.14 eV), but the gaps to the lower branches are much smaller: 0.07, 0.04, 0.06, and the total width of the resulting "superband" is 1.1 eV.

### S7. Side chains sampling

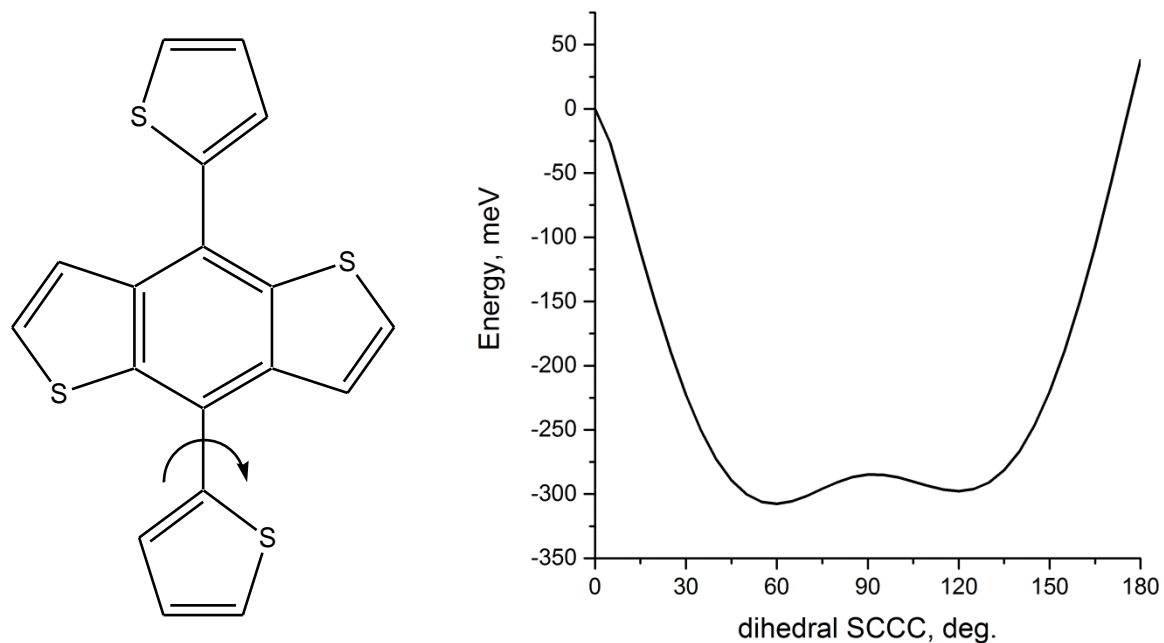


Fig. S12. 1D PES section for di(1,4)thiophenylbenzodithiophene molecule corresponding to internal rotation of on thiophene ring around benzodithiophene core.

Table S21. Changes (related to planar conformation) in HOMO/LUMO levels (in eV) induced by internal rotation of thiophene ring related to benzodithiophene unit.

dihedral, deg.	HOMO, eV		LUMO, eV	
	gas	clf	gas	clf
benzodithiophene molecule				
no side thiophenes	-0.31	-0.25	0.68	0.74
0.0	0.00	0.00	0.00	0.00
59.4	-0.08	-0.09	0.31	0.31
90.0	-0.17	-0.18	0.38	0.38
benzodithiophene-centered oligomer of P4				
no side thiophenes	-0.02	-0.01	0.01	0.02
0.0	0.00	0.00	0.00	0.00
59.4	0.01	-0.02	0.02	0.01
90.0	0.00	-0.04	0.02	0.01

## S8. Structural properties

Table S22. Structural descriptors and basic electronic properties of ideal polymers. The 'linearity RMS' is defined as RMS deviation of centers of bridging bonds from ideal linear polymer in the energetically lowest conformation (for example, it is zero for polythiophene). The 'linearity penalty' is defined as the energy penalty per unit length to make the most linear conformer. Note that for the rod group pmcm the translation period is two times larger than the polymer repeating unit.

Descriptor	DTBTBT	DTFTFT	DT2BTBT2	DT2FTFT2	DT2FT2FT2	T2FDFT2	DTBT	DTFT	TFT	T2FT2
	P1	P2	P3	P4	Q1	Q2	U1	U2	T1	T2 <sup>a)</sup>
Rod group	pmcm	pmcm	pmcm	pmcm	p112/m	p112/m	pmcm	pmcm	pmcm	pm11
Repeating unit length (Å)	24.2	25.0	33.4	34.2	40.0	41.1	18.9	19.2	12.0	20.0
Linearity RMS (Å)	5.36	5.00	4.82	4.25	0.93	0.49	2.97	2.81	0.86	0.30
-LUMO (eV)	2.03	2.11	1.98	2.07	2.02	2.05	1.93	2.01	2.10	1.98
-HOMO (eV)	6.10	6.20	6.04	6.12	6.10	6.16	6.11	6.18	6.12	6.00
-EA in clf (eV) <sup>b)</sup>	2.58	2.62	2.51	2.56	-	-	2.54	2.59	-	-
IP in clf (eV) <sup>b)</sup>	5.55	5.66	5.52	5.61	-	-	5.57	5.64	-	-
HOMO-LUMO gap (eV)	4.07	4.09	4.06	4.05	4.08	4.11	4.18	4.17	4.03	4.01

<sup>a)</sup> Not the lowest-energy conformation.

<sup>b)</sup> Estimations are obtained by the following expression: IP (polymer) = [IP + HOMO](oligomer) - HOMO(polymer). -EA is estimated accordingly.

Linearity penalty estimation made for **P4** structure is 1.45 meV/ Å.

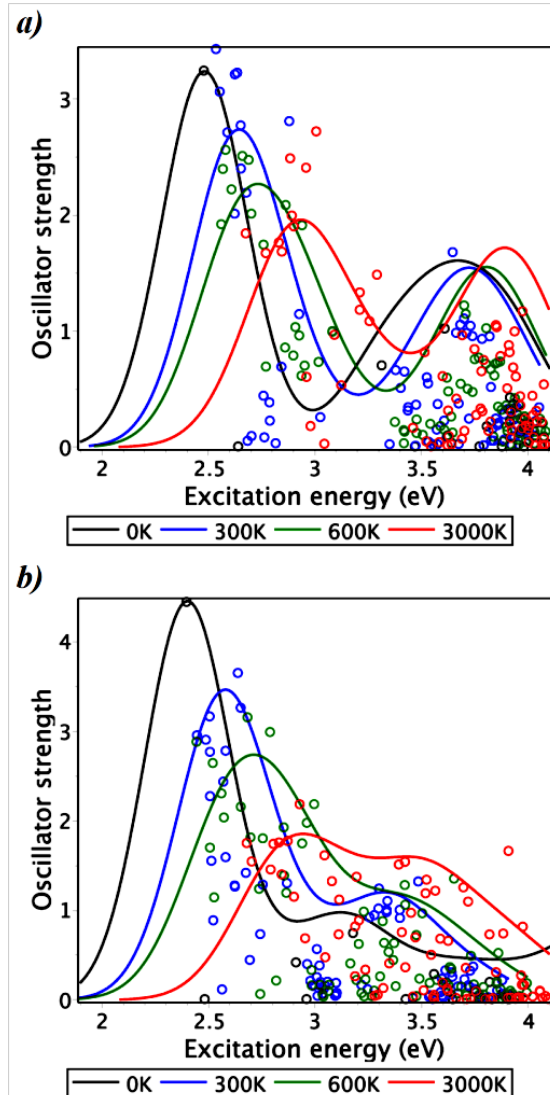


Fig. S13. Conformational sampling of (a) **P1** and (b) **P3** absorption spectra in solution in the independent rotation approximation. More specifically, we optimize the planar conformation of the donor-centered oligomer of 13 rigid building blocks (TBTBT2DT2BTBT) without side chains, then sample all 12 flexible dihedrals in Boltzmann statistics (10 samples) using PES of the corresponding dimers, and calculate 8 excited states for each conformer in the simulated ensemble (line broadening is 0.2 eV). The temperature of ensemble is given in the legends: here 0K corresponds to the fully planar conformer, whereas 3000K corresponds to almost random distribution of dihedrals. Since side chains and polymer self-intersections effectively increase disorder, 300K sampling gives only the lower limit for the effects of disorder in a solution. Also, as discussed in the manuscript inclusion of additional thiophenes makes **P3** polymer more flexible than **P1**, which is clearly seen on this picture.

## References

- [1] M. Wang, X. Hu, P. Liu, W. Li, X. Gong, F. Huang, Y. Cao, Donor–Acceptor Conjugated Polymer Based on Naphtho[1,2-*c*:5,6-*c*]bis[1,2,5]thiadiazole for High-Performance Polymer Solar Cells, *J. Am. Chem. Soc.* 133 (2011) 9638–9641. doi:[10.1021/ja201131h](https://doi.org/10.1021/ja201131h).
- [2] A.V. Akkuratov, D.K. Susarova, L.N. Inasaridze, P.A. Troshin, The effect of the fluorine loading on the optoelectronic and photovoltaic properties of (X-DADAD-)<sub>n</sub>-type donor-acceptor copolymers with the benzothiadiazole A units: Effect of fluorine loading on (X-DADAD-)<sub>n</sub>-type copolymers, *Phys. Status Solidi RRL.* 11 (2017) 1700087. doi:[10.1002/pssr.201700087](https://doi.org/10.1002/pssr.201700087).
- [3] A.V. Akkuratov, D.K. Susarova, Y.L. Moskvin, D.V. Anokhin, A.V. Chernyak, F.A. Prudnov, D.V. Novikov, S.D. Babenko, P.A. Troshin, A strong influence of the positions of solubilizing alkyl side chains on optoelectronic and photovoltaic properties of TTBTBTT-based conjugated polymers, *J. Mater. Chem. C.* 3 (2015) 1497–1506. doi:[10.1039/C4TC02432J](https://doi.org/10.1039/C4TC02432J).
- [4] A.V. Akkuratov, F.A. Prudnov, L.N. Inasaridze, P.A. Troshin, Synthesis of the (X-DADAD)<sub>n</sub>-type conjugated polymers with 2,1,3-benzoxadiazole acceptor blocks and their application in organic solar cells, *Tetrahedron Letters.* 58 (2017) 97–100. doi:[10.1016/j.tetlet.2016.11.107](https://doi.org/10.1016/j.tetlet.2016.11.107).
- [5] C.L. Chochos, N. Leclerc, N. Gasparini, N. Zimmerman, E. Tatsi, A. Katsouras, D. Moschovas, E. Serpetzoglou, I. Konidakis, S. Fall, P. Lévêque, T. Heiser, M. Spanos, V.G. Gregoriou, E. Stratakis, T. Ameri, C.J. Brabec, A. Avgeropoulos, The role of chemical structure in indacenodithienothiophene-*alt*-benzothiadiazole copolymers for high performance organic solar cells with improved photo-stability through minimization of burn-in loss, *J. Mater. Chem. A.* 5 (2017) 25064–25076. doi:[10.1039/C7TA09224E](https://doi.org/10.1039/C7TA09224E).
- [6] O. Ostroverkhova, Organic Optoelectronic Materials: Mechanisms and Applications, *Chem. Rev.* 116 (2016) 13279–13412. doi:[10.1021/acs.chemrev.6b00127](https://doi.org/10.1021/acs.chemrev.6b00127).
- [7] J. Zhao, Y. Li, G. Yang, K. Jiang, H. Lin, H. Ade, W. Ma, H. Yan, Efficient organic solar cells processed from hydrocarbon solvents, *Nat Energy.* 1 (2016) 15027. doi:[10.1038/nenergy.2015.27](https://doi.org/10.1038/nenergy.2015.27).
- [8] C. Duan, A. Furlan, J.J. van Franeker, R.E.M. Willems, M.M. Wienk, R.A.J. Janssen, Wide-Bandgap Benzodithiophene-Benzothiadiazole Copolymers for Highly Efficient Multijunction Polymer Solar Cells, *Adv. Mater.* 27 (2015) 4461–4468. doi:[10.1002/adma.201501626](https://doi.org/10.1002/adma.201501626).
- [9] A. Zhugayevych, S. Tretiak, Theoretical Description of Structural and Electronic Properties of Organic Photovoltaic Materials, *Annu. Rev. Phys. Chem.* 66 (2015) 305–330. doi:[10.1146/annurev-physchem-040214-121440](https://doi.org/10.1146/annurev-physchem-040214-121440).
- [10] J. Frisch, G. W. Trucks, H. B. Schlegel, G. E. Scuseria, M. A. Robb, J. R. Cheeseman, G. Scalmani, V. Barone, G. A. Petersson, H. Nakatsuji, X. Li, M. Caricato, A.

Marenich, J. Bloino, B. G. Janesko, R. Gomperts, B. Mennucci, H. P. Hratchian, J. V. Ortiz, A. F. Izmaylov, J. L. Sonnenberg, D. Williams-Young, F. Ding, F. Lipparini, F. Egidi, J. Goings, B. Peng, A. Petrone, T. Henderson, D. Ranasinghe, V. G. Zakrzewski, J. Gao, N. Rega, G. Zheng, W. Liang, M. Hada, M. Ehara, K. Toyota, R. Fukuda, J. Hasegawa, M. Ishida, T. Nakajima, Y. Honda, O. Kitao, H. Nakai, T. Vreven, K. Throssell, J. A. Montgomery, Jr., J. E. Peralta, F. Ogliaro, M. Bearpark, J. J. Heyd, E. Brothers, K. N. Kudin, V. N. Staroverov, T. Keith, R. Kobayashi, J. Normand, K. Raghavachari, A. Rendell, J. C. Burant, S. S. Iyengar, J. Tomasi, M. Cossi, J. M. Millam, M. Klene, C. Adamo, R. Cammi, J. W. Ochterski, R. L. Martin, K. Morokuma, O. Farkas, J. B. Foresman, and D. J. Fox, Gaussian, Inc., Wallingford CT, 2016.

- [11] D. Jacquemin, C. Adamo, Bond Length Alternation of Conjugated Oligomers: Wave Function and DFT Benchmarks, *J. Chem. Theory Comput.* 7 (2011) 369–376. doi:[10.1021/ct1006532](https://doi.org/10.1021/ct1006532).
- [12] I.H. Nayyar, E.R. Batista, S. Tretiak, A. Saxena, D.L. Smith, R.L. Martin, Role of Geometric Distortion and Polarization in Localizing Electronic Excitations in Conjugated Polymers, *J. Chem. Theory Comput.* 9 (2013) 1144–1154. doi:[10.1021/ct300837d](https://doi.org/10.1021/ct300837d).
- [13] A. Zhugayevych, O. Postupna, H.-L. Wang, S. Tretiak, Modification of optoelectronic properties of conjugated oligomers due to donor/acceptor functionalization: DFT study, *Chemical Physics*. 481 (2016) 133–143. doi:[10.1016/j.chemphys.2016.09.009](https://doi.org/10.1016/j.chemphys.2016.09.009).
- [14] A. Zhugayevych, O. Mazaleva, A. Naumov, S. Tretiak, Lowest-Energy Crystalline Polymorphs of P3HT, *J. Phys. Chem. C* 122 (2018) 9141–9151. doi:[10.1021/acs.jpcc.7b11271](https://doi.org/10.1021/acs.jpcc.7b11271).
- [15] Y. Takano, K.N. Houk, Benchmarking the Conductor-like Polarizable Continuum Model (CPCM) for Aqueous Solvation Free Energies of Neutral and Ionic Organic Molecules, *J. Chem. Theory Comput.* 1 (2005) 70–77. doi:[10.1021/ct049977a](https://doi.org/10.1021/ct049977a).
- [16] M. Cossi, N. Rega, G. Scalmani, V. Barone, Energies, structures, and electronic properties of molecules in solution with the C-PCM solvation model, *J. Comput. Chem.* 24 (2003) 669–681. doi:[10.1002/jcc.10189](https://doi.org/10.1002/jcc.10189).
- [17] V. Barone, M. Cossi, Quantum Calculation of Molecular Energies and Energy Gradients in Solution by a Conductor Solvent Model, *J. Phys. Chem. A* 102 (1998) 1995–2001. doi:[10.1021/jp9716997](https://doi.org/10.1021/jp9716997).